

# Assignment 1 – Experimental Modal Analysis

Prof. R. Corradi, Dr. I. La Paglia

## Contents

Part A: Cantilever beam	3
Introduction	3
A.1. Natural frequencies and mode shapes	4
A.2. Frequency Response Functions	7
A.3. Modal parameter identification	10
A.4. Quality of the identification	12
A.5. Identified parameters and mode shapes	20
Part B: Experimental Modal Analysis of a light rail wheel	24
Introduction	24
B.1. Modal parameter identification	25
B.2. Quality of the identification	29
B.3. Identified parameters and mode shapes	39

## Part A: Cantilever beam

### Introduction

In this first part of the project the cantilever beam dynamic is analyzed using MATLAB to model its behavior.

This part is organized in the following manner:

1. Computation of natural frequencies and mode shapes
2. Computation of the Frequency Response Function for different input and output positions
3. Identification of modal parameters FRF-based multi-curve fitting method
4. Analysis of the results of the identified parameters
5. Mode shapes given by the identified parameters

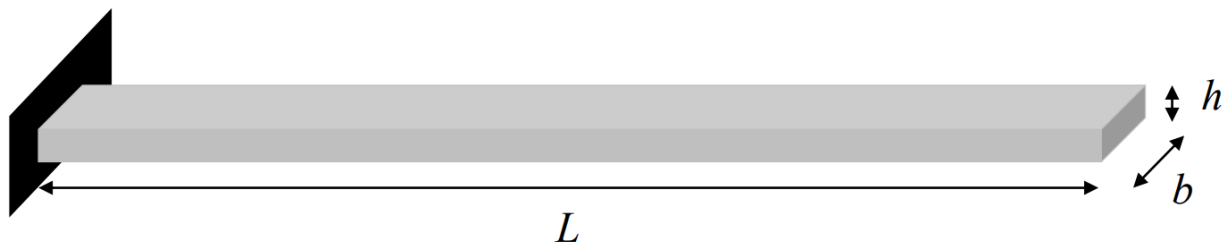


Figure 1: cantilever beam

Figure 1 shows the cantilever beam, subject of the present study. It is an aluminum beam with a rectangular cross-section, with the following properties.

#### Beam properties

Parameters	symbol	unit	value
Length	$L$	mm	1200
Thickness	$h$	mm	8
Width	$b$	mm	40
Density	$\rho$	Kg/m <sup>3</sup>	2700
Young's Modulus	$E$	GPa	58

## A.1. Natural frequencies and mode shapes

### *Standing wave solution*

To compute the natural frequencies and the mode shapes of the cantilever beam, it was firstly imposed the standing wave solution for the vertical vibration  $w(x,t)$  of a slender beam undergoing bending vibration.

$$w(x,t) = \Phi(x) G(t) = [A \cos(\gamma x) + B \sin(\gamma x) + C \cosh(\gamma x) + D \sinh(\gamma x)] \cos(\omega t + \varphi)$$

Wavenumber equation:

$$\gamma^4 = \frac{m \omega^2}{EJ}$$

- m: mass per unit length
- $\omega$ : natural frequency
- E: Young's Modulus
- J: ( $J = bh^3/12$ ) cross-section area moment of inertia of the beam

### *Boundary conditions*

Four boundary conditions must be applied to evaluate the unknown coefficients A, B, C, D. Moreover, the solution must be valid for any time t, therefore the shape function part of the standing wave solution has been considered only.

1) Displacement constraint at the left end of the beam ( $x=0$ )

$$w(0, t) = A + C = 0$$

2) Rotation constraint at  $x=0$

$$\frac{\partial w}{\partial x}(0, t) = \gamma(B + D) = 0$$

3) Vertical force equilibrium at beam end ( $x=L$ ), by considering the shear force T

$$T(L, t) = EJ \frac{\partial^3 w}{\partial x^3}(L, t) = 0$$

Which leads to:  $A \sin(\gamma L) - B \cos(\gamma L) + C \sinh(\gamma L) + D \cosh(\gamma L) = 0$

4) Moment equilibrium at  $x=L$

$$M = EJ \frac{\partial^2 w}{\partial x^2}(L, t) = 0$$

Which leads to:  $-A \cos(\gamma L) - B \sin(\gamma L) + C \cosh(\gamma L) + D \sinh(\gamma L) = 0$

### *Matrix formulation*

Considering the vector of our unknown given by the boundary conditions, they can be rewritten in the following matrix form.

$$\begin{bmatrix} 1 & 0 & 1 & 0 \\ 0 & 1 & 0 & 1 \\ \sin(\gamma L) & -\cos(\gamma L) & \sinh(\gamma L) & \cosh(\gamma L) \\ -\cos(\gamma L) & -\sinh(\gamma L) & \cosh(\gamma L) & \sinh(\gamma L) \end{bmatrix} \begin{bmatrix} A \\ B \\ C \\ D \end{bmatrix} = \begin{bmatrix} 0 \\ 0 \\ 0 \\ 0 \end{bmatrix}$$

Therefore, by naming  $H(\omega)$  the first matrix:

$$[H(\omega)]z = 0$$

Considering the non-trivial solution

$$\det[H(\omega)] = 0$$

#### *Solution of the characteristic equation*

To solve this equation the matrix  $H(\omega)$ , and consequently its determinant, is written in MATLAB as an anonymous function of the variable gamma. Then using the Newton Method, the values of gamma that make the determinant of  $H(\omega)$  equal to zero are found.

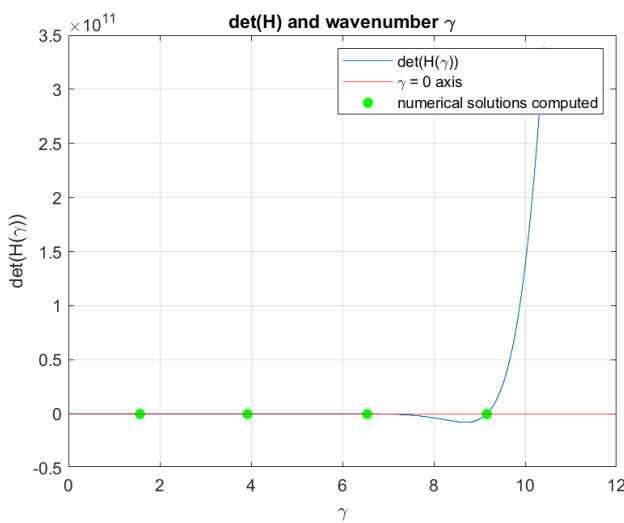


Figure 2: Value of the  $\det(H)$  against  $\gamma$

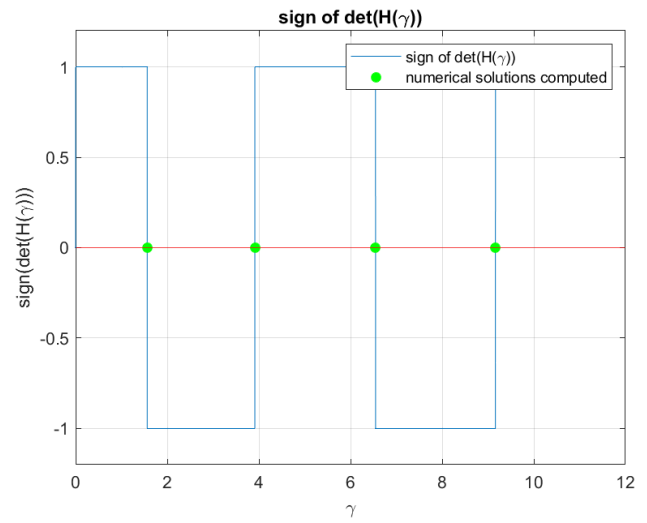


Figure 3: sign of  $\det(H)$  against  $\gamma$

Figure 2 displays the value of the determinant of the coefficient matrix, in function of the wavenumber, scaled by the beam length. In green are represented the dots corresponding to the wave number which make the determinant equal to zero.

Figure 3 displays the sign of the determinant presented in figure 2, from this plot is easy to confirm that the function is passing in zero in the identified points.

With the wavenumber equation presented previously, it is possible to convert the wavenumber identified with the Newton Method into natural frequencies. So, the computed natural frequencies for the considered beam are the following:

	Mode 1	Mode 2	Mode 3	Mode 4
$\omega$	4.5038 Hz	28.2249 Hz	79.0306 Hz	154.8684 Hz

#### *Mode shape computation*

To compute the mode shapes, it is necessary to get the A, B, C, D coefficients for the assigned natural frequencies. To achieve this, the previous system of equations, obtained through the imposition of the boundary conditions is considered. Since the determinant of the matrix of coefficients has been imposed as null, the matrix is now singular, therefore the system is defined apart from a scaling factor. Hence, the A coefficient for the standing wave solution has been imposed unitary. To obtain the exact values of B, C, D in relation to A = 1 it's now considered the same system as before, but without the first row. The known term

becomes the opposite of the first column of the coefficient matrix, which then gets cancelled. The resulting system is shown below.

$$\begin{bmatrix} 1 & 0 & 1 \\ -\cos(\gamma L) & \text{Sinh}(\gamma L) & \text{Cosh}(\gamma L) \\ -\sinh(\gamma L) & \text{Cosh}(\gamma L) & \text{Sinh}(\gamma L) \end{bmatrix} \begin{bmatrix} B \\ C \\ D \end{bmatrix} = \begin{bmatrix} 0 \\ -\sin(\gamma L) \\ \cos(\gamma L) \end{bmatrix}$$

The shape function  $\phi_i(x)$  of the transverse vibration for the standing wave solution has been, now, defined for all the first four vibration modes.

$$\Phi_i(x) = A_i \cos(\gamma_i x) + B_i \sin(\gamma_i x) + C_i \text{Cosh}(\gamma_i x) + D_i \text{Sinh}(\gamma_i x)$$

The first four mode shapes are plotted below in fig.4., after being scaled by their maximum value.

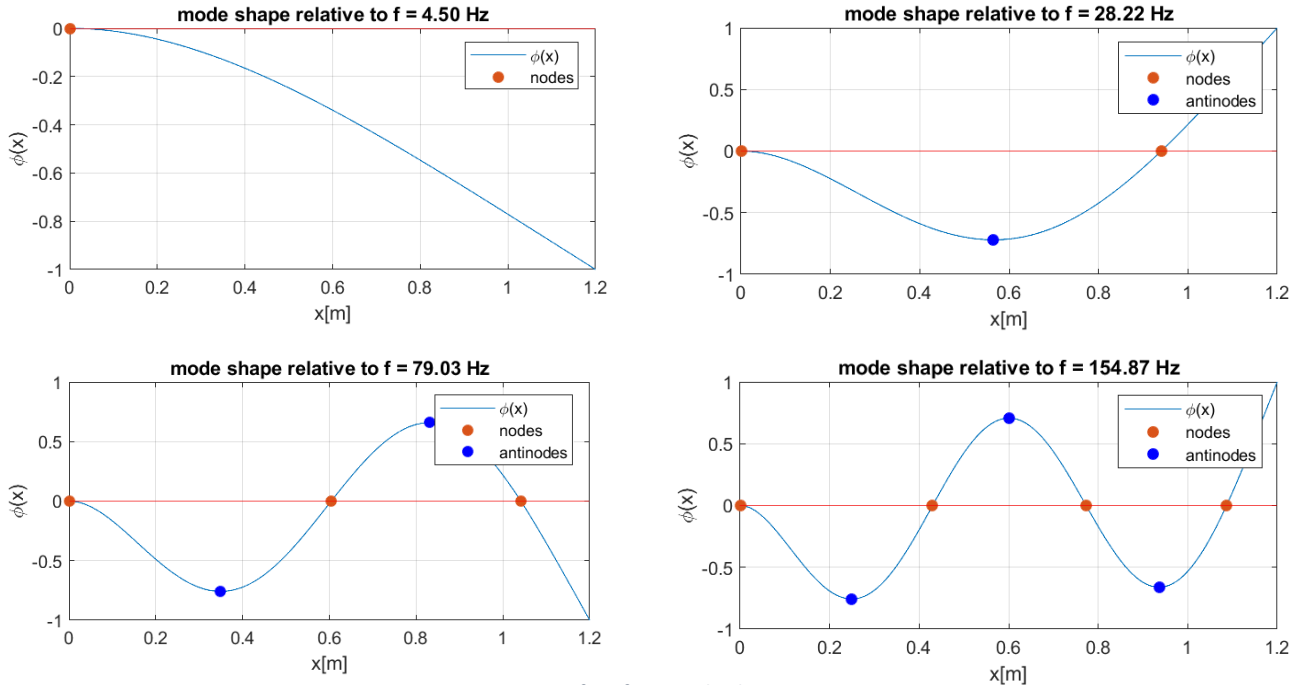


Figure 4: first four mode shapes

Finally, considering  $n = 4$  (first four modes), the standing wave solution for the vertical vibration  $w(x,t)$  of a slender beam undergoing bending vibration is:

$$w(x,t) = \sum_i^4 \Phi_i(x) G_i(t)$$

$$w(x,t) = \sum_i^4 \{ [A_i \cos(\gamma_i x) + B_i \sin(\gamma_i x) + C_i \text{Cosh}(\gamma_i x) + D_i \text{Sinh}(\gamma_i x)] \cos(\omega_i t + \varphi) \}$$

## A.2. Frequency Response Functions

### Frequency response function

The frequency response function evaluates the response of the system to a given input force. In this specific case the input force is  $F_k(t)$  and the displacement is  $w(x_j, t)$ .



Figure 5: Transverse vibration  $w(x_j, t)$  for a harmonic force input  $F_k(t)$

To compute the FRF it is necessary to implement this following formula, which comes from the modal superposition approach:

$$G_{jk}(\Omega) = \sum_{i=1}^n \frac{\Phi_i(x_j) \Phi_i(x_k) / m_i}{-\Omega^2 + j2\xi_i\omega_i\Omega + \omega_i^2}$$

In this formula the contributions of each mode shape are summed up to evaluate the final response of the system. The dependency on the position of the input force and the resulting vibration are given by  $x_j$  and  $x_k$ , respectively the position of interest of displacement and the position where the force is applied. Note that for the reciprocity principle, interchanging the point of application of the force and the measurement point doesn't affect the FRF.

In our specific case:

- $n = 4$ , as only the first four mode shapes are considered
- Damping ratio is chosen in the order of 1%
- $\omega_i$  are the natural frequencies computed in item A.1.
- The modal mass  $m_i$  is computed as it follows:  $m_i = \int_0^L m \phi_i^2(x) dx$  (computed in MATLAB with the function 'trapz', trapezoidal method)

### Analysis of peculiar cases

1.  $x_j = 0.2 \text{ m}$ ,  $x_k = 1.2 \text{ m}$  (generic FRF)

In this first case, the choice of input and output location is random, to give a general idea of what an FRF looks like for the cantilever beam in subject. Fig.6 shows a typical FRF, with four peaks (and four phase  $-\pi$  delays) in correspondence of the first four natural frequencies (resonance regions) and a well distributed behavior among those.

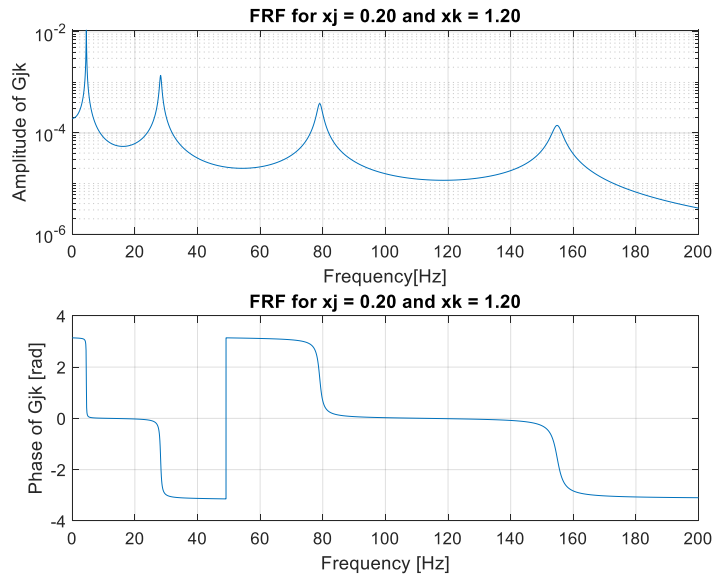


Figure 6: General case FRF

## 2. $x_j = 1.2 \text{ m}$ , $x_k = 1.2 \text{ m}$ (co-located response)

In the second case input and output locations coincide, showing the results of a co-located FRF. In fact, input and output correspond to the end of the beam, where vibrations are the maximum for all modes. The typical behavior of a co-located FRF is, therefore, observed in fig.7. Peaks are sharper and higher with respect to “case 1”, but most importantly modes appear to be de-coupled, by having anti-resonances (tending to null amplitude and by shifting phase by  $+π$ ) in between all resonance regions.

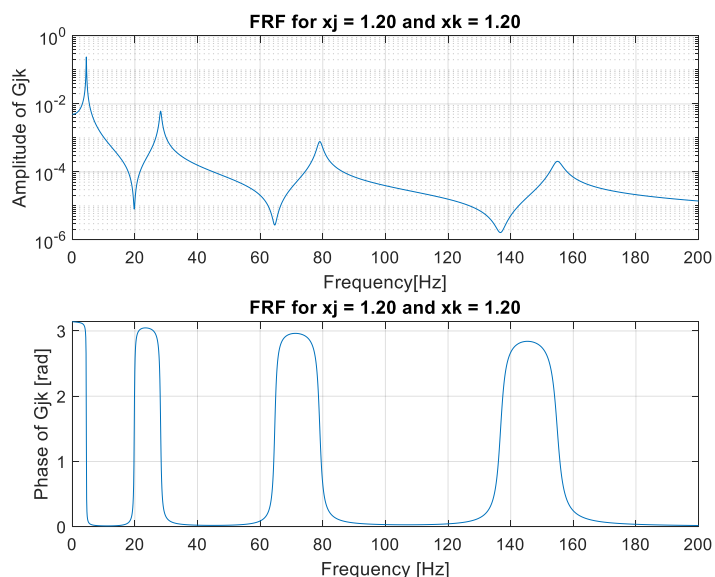


Figure 7: Co-located FRF

3.  $x_j = 1.2 \text{ m}$ ,  $x_k = 0.2 \text{ m}$  (reciprocity principle)

In the third case, input and output positions are the same as the first case but swapped. Fig.8 shows that the FRF obtained in this case and the first one is the same, demonstrating the reciprocity principle. In fact, being the formula for the shape function  $\Phi(x)$  the same independently from the input/output location and, having the  $G(\Omega)$  formula the two separate contributions simply multiplied by each other, this behavior is explained.

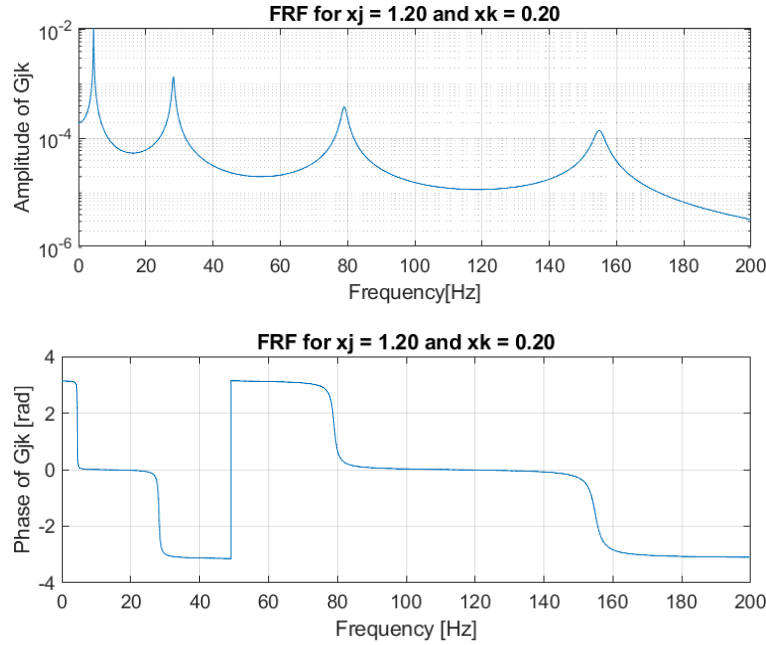


Figure 8: reciprocity principle

4.  $x_j = 0.94 \text{ m}$ ,  $x_k = 1.2 \text{ m}$  (uncontrollable mode)

The fourth case highlights the effect of the uncontrollability of one mode. The measurement point is placed in correspondence of a node of the second vibration mode. This leads to the cancellation of the contribution of the second mode to the overall frequency response, as it is shown in fig.9.

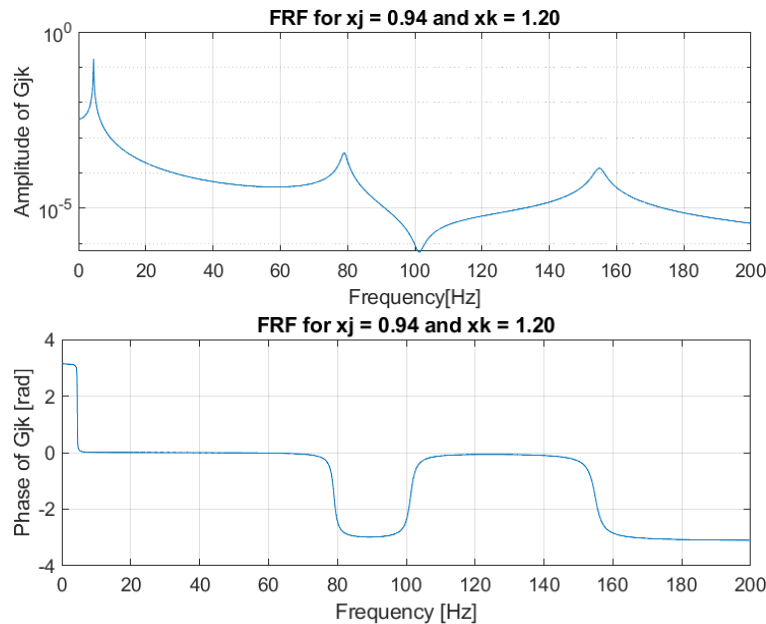


Figure 9

### A.3. Modal parameter identification

Section A.3 outlines the procedure followed to identify the modal parameters of the first four modes. This was achieved through the implementation of the FRF-based-multi-mode curve fitting method for a single mode at a time ( $n=1$ ). The formula represents the reference for this algorithm and its parameters are the final targets to obtain, considering  $n=i$ , for  $i = 1, 2, 3, 4$ .

$$G_{jk}^{NUM}(\Omega) = \sum_{i=1}^n \frac{A_{jk}^{(i)}}{-\Omega^2 + j2\xi_i\omega_i\Omega + \omega_i^2} + \frac{R_{jk}^L}{\Omega^2} + R_{jk}^H$$

$A_{jk}$  is the element of the modal vector representing the mode shape of the considered mode at the given  $x_j$ ,  $x_k$ .  $\xi_i$  is the damping ratio.  $\omega_i$  is the natural frequency of the considered mode. Finally, the  $R_{jk}$  terms are residuals that represent, instead, the contributions from the higher (H) and lower (L) order modes peaks, that are not included in the selected frequency band.

The previously described parameters are obtained through a least square minimization process of an error function  $\epsilon$  which represents the difference between the experimental (in this case simulation) and the numerical FRFs, as it is described with the formulation below.

$$\epsilon = \sum_{r=1}^N \sum_{s=1}^M (G_r^{EXP}(\Omega_s) - G_r^{NUM}(\Omega_s)) (G_r^{EXP}(\Omega_s) - G_r^{NUM}(\Omega_s))^*$$

Here,  $G^{EXP}(\Omega_s)$ , represents the matrix containing the experimentally obtained (simulated) FRFs. The matrix has  $M$  rows corresponding to the length of the frequency vector  $\Omega_s$  over which the FRFs are evaluated and  $N$  columns representing the number of FRFs which are considered per set.  $G^{NUM}(\Omega_s)$  is the numerical estimation of the FRFs around a specific natural frequency around a certain  $\omega_i$ . In this context,  $G^{NUM}(\Omega_s)$  is a MATLAB function that takes in input the frequency range  $\Omega_s$  and a vector of  $2+3N$  unknowns, corresponding to  $\omega_i$ ,  $\xi_i$  and  $N A_{jk}^H$ ,  $R_{jk}^L$  and returns as an output the evaluation of the FRF numerically computed.

The frequency range  $\Omega_s$ , used for computing the FRFs varies depending on the mode under consideration. This range is chosen as a subset of the overall frequency spectrum, ensuring it contains only the natural frequency corresponding to the specific mode being analyzed.

To determine this range, we first identified an approximate value for the natural frequency by examining the plot of natural frequencies obtained in the previous step. The lower limit of the range was set slightly below this identified natural frequency, while the upper limit was defined as 6 Hz above the lower limit. This approach ensures that the range adequately captures the behavior around the natural frequency for each mode.

To perform the least square minimization, the built-in “lsqnonlin()” MATLAB function has been adopted for each modal parameter identification. This function takes as input the error function  $\epsilon$ , that must be minimized and a vector containing  $2+3N$  initial guesses. It returns as an output the vector with the optimal  $2+3N$  values previously introduced.

To ensure reliable initial guesses, different methods were implemented and were repeated for each mode characterization.

To determine the first guess for the natural frequency ( $\omega_{i\_0}$ ), it was taken the value of frequency corresponding to the highest value in amplitude of the experimental (simulated) FRF per each mode.

A good approximation for the damping ratio was identified from the slope of the phase diagram ( $\Phi$ ), in correspondence with  $\omega_i$  (which is inversely proportional to  $\xi_i$ ).

$$\xi_{i\_0} = \frac{1}{\omega_i \cdot \left. \frac{\partial \Phi_i}{\partial \Omega} \right|_{\Omega=\omega_i}}$$

The  $A_{jk}$  parameter which represents the modal vector evaluated in the  $x_j, x_k$  positions, is obtained by multiplying the negative of the imaginary part of the resonance peak value times twice the initial guess for the damping ratio and the squared natural frequency.

$$A_{jk}^i = -2 \operatorname{Im}(G_{jk}^{EXP}(\omega_{i\_0})) \xi_{i\_0} \omega_{i\_0}^2$$

Finally, the  $2N$  initial values for the computation of the residuals have been imposed null.

Having now defined all the parameters and all the functions necessary for the modal parameter identification, through the single-mode curve fitting method, the algorithm has been put into work. The results are shown in the next chapters.

## A.4. Quality of the identification

The fourth item of part A of the first assignment requires checking the quality of the identification, comparing the identified FRFs and the ones numerically computed.

To carry out the modal parameter identification of each mode a set of three “experimental” FRFs was chosen with the following input and output locations:

- 1)  $X_j = 0.2 \text{ m}$        $X_k = 1.2 \text{ m}$
- 2)  $X_j = 0.9401 \text{ m}$      $X_k = 1.2 \text{ m}$  ( $X_j$  here is in position of a node)
- 3)  $X_j = 1.2 \text{ m}$        $X_k = 1.2 \text{ m}$

The choice of the  $X_j$  were done to show different cases:

- Case 2 is a non-observable case: sensor is located at a node
- Case 3 is a collocated case: sensor and force are in the same location

Then for each mode a frequency range was chosen, and it was plotted the experimental FRFs with the numerical FRF computed in that specific frequency range.

### Mode 1

Figures 10, 11, and 12 illustrate the excellent accuracy of the method comparing the data obtained from the numerical FRF (red) with the overall experimental FRF (blue). Each graph shows the first mode peak for each  $X_j, X_k$  pair written in the title. This is to remark how reliable is the single-mode curve fitting method in this region, considering also that it takes into account contributions from lower and higher order modes.

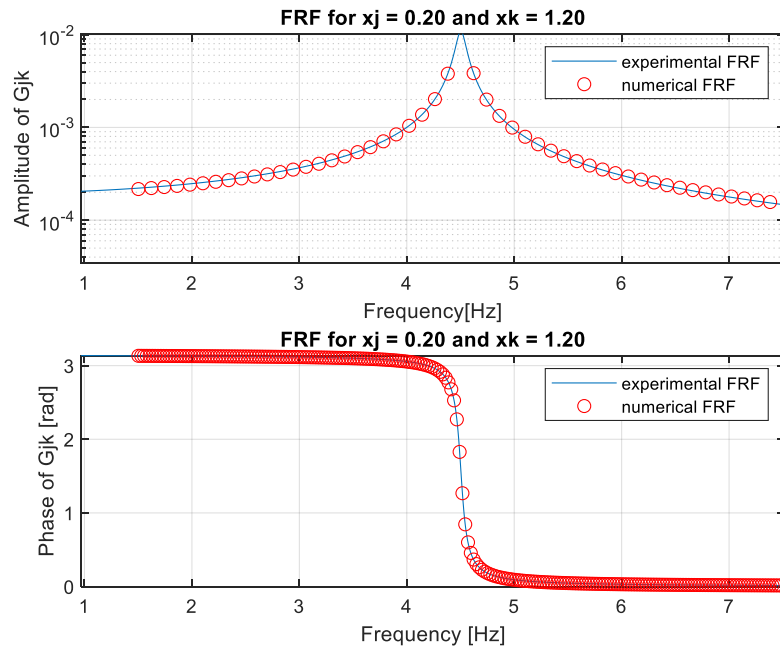


Figure 10: First mode  $X_j=0.20$

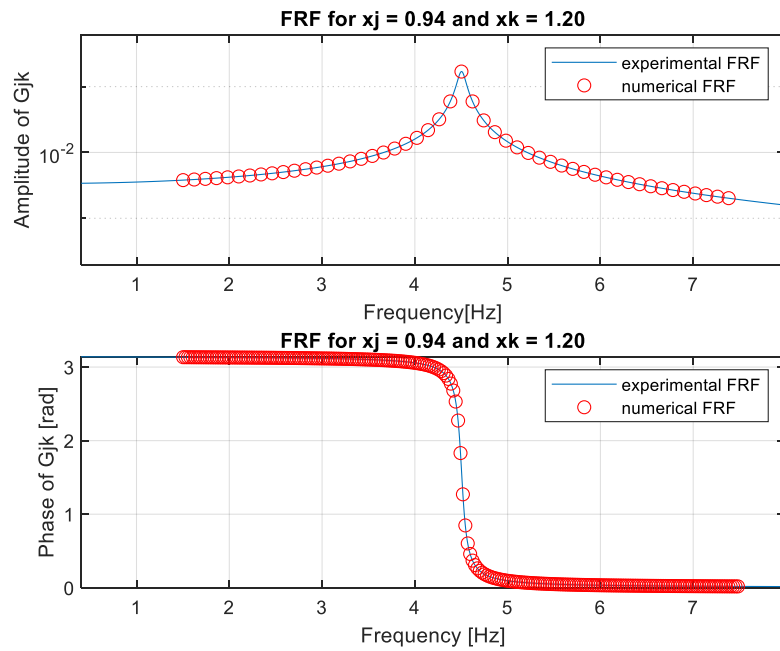


Figure 11: First mode  $X_j=0.94$

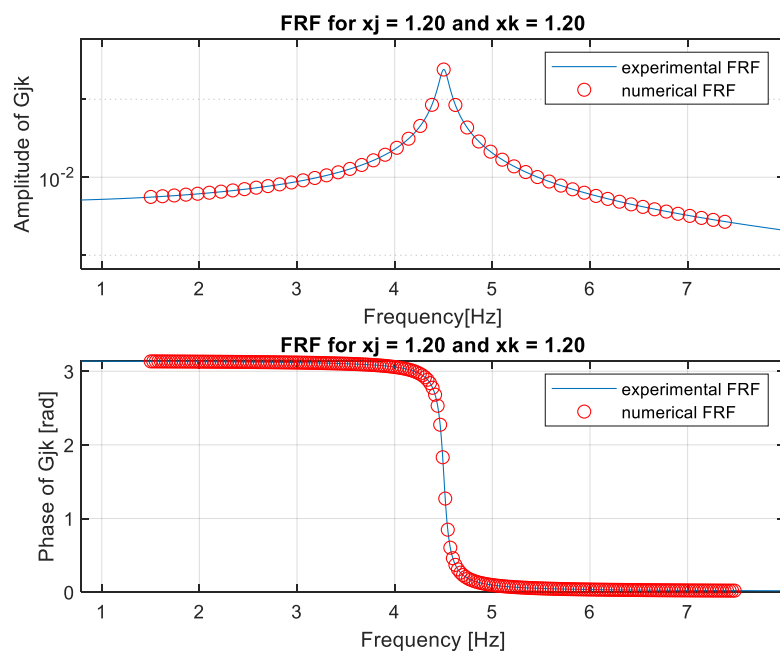


Figure 12: First mode  $X_j=1.2$

Fig.13 shows a particular comparison between the first FRF of the simulated set (blue) with its identified counterpart (red), to have a more global idea of the results for mode 1 in the specific case of  $X_j=1.20$  and  $X_k=1.20$ . This case is called “collocated FRF”, meaning that the sensor and the force are in the same position and, as we can see also from the graph, it is characterized by a alternation of resonance and anti-resonance peaks.

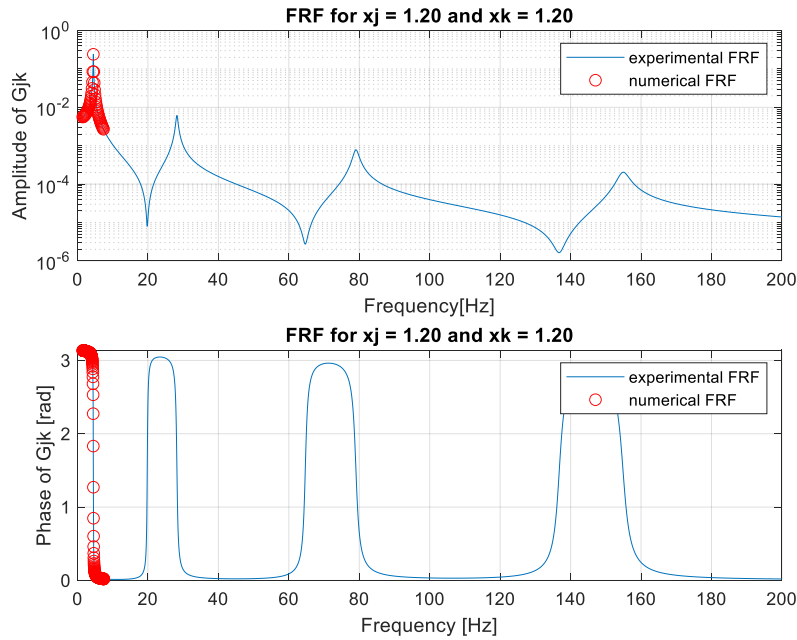


Figure 13: Collocated FRF

### Mode 2

Each graph displays the first mode peak for the  $X_j$ ,  $X_k$  pair specified in the title

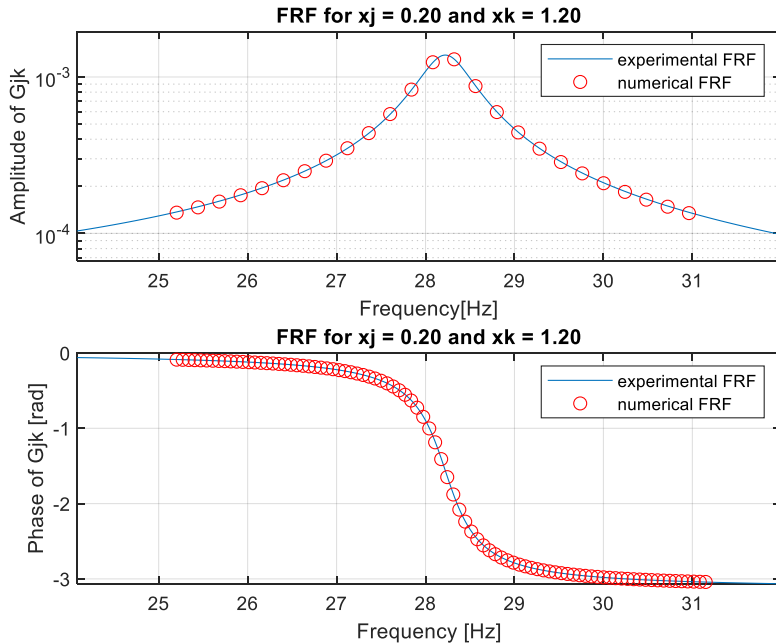


Figure 14: second mode  $X_j=0.20$

In  $X_j=0.94$  we have the non-observable case, so the numerical estimation is not able to compute the values of the resonance peak, because the peak does not exist.

In Figure 16, we can see a slight misalignment on the left and right side of the peak, probably due to the presence of the close antiresonance peak before the resonance peak, the alternation of the resonance and antiresonance peaks are caused by the collocated FRF as discussed previously.

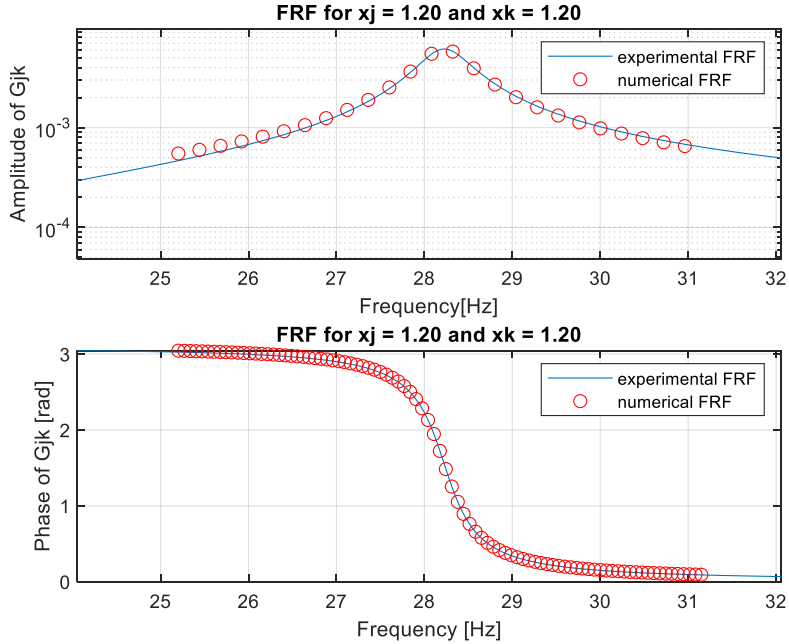


Figure 15: Second mode  $X_j=1.20$

### Mode 3

Each graph displays the first mode peak for the  $X_j$ ,  $X_k$  pair specified in the title.

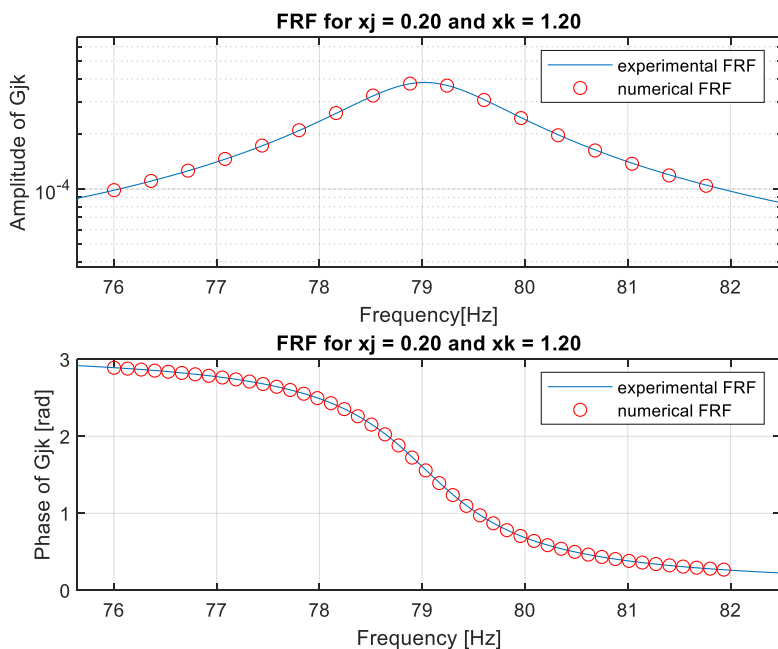


Figure 16: Third mode  $X_j=0.20$

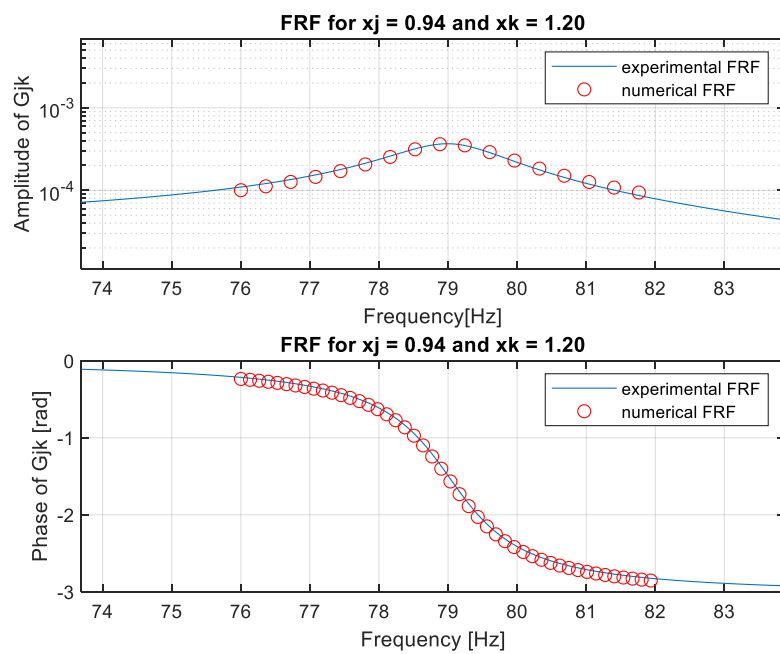


Figure 17: Third mode  $X_j=0.94$

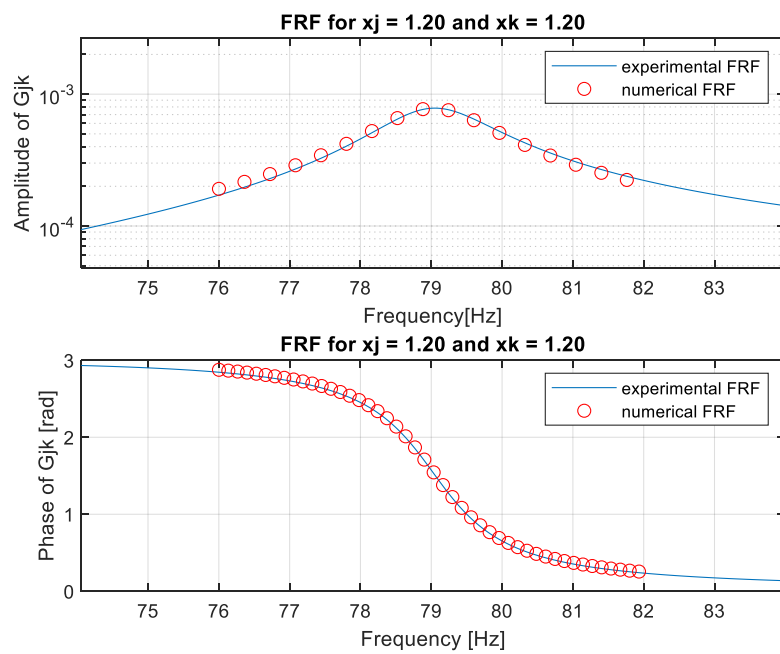


Figure 18: Third mode  $X_j=1.20$

#### Mode 4

Each graph displays the first mode peak for the  $X_j$ ,  $X_k$  pair specified in the title.

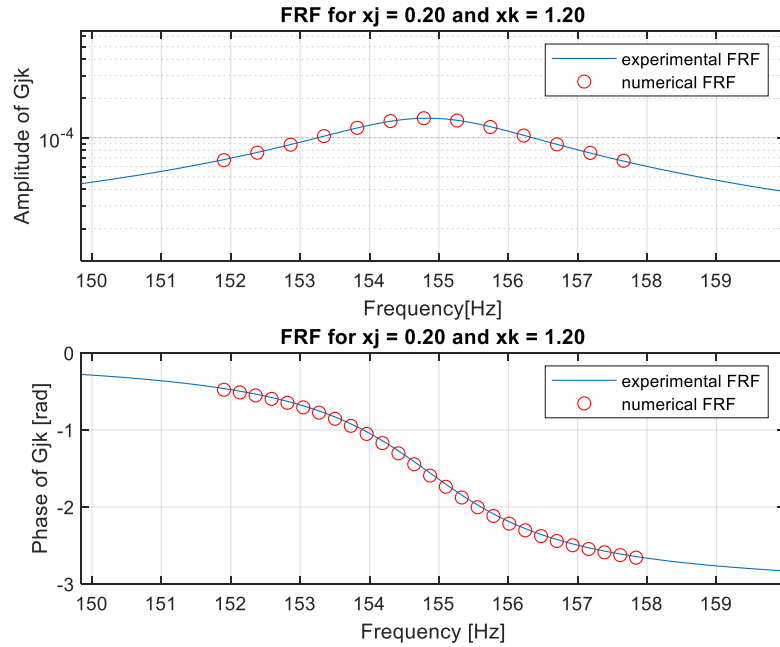


Figure 19: Fourth mode  $X_j=0.20$

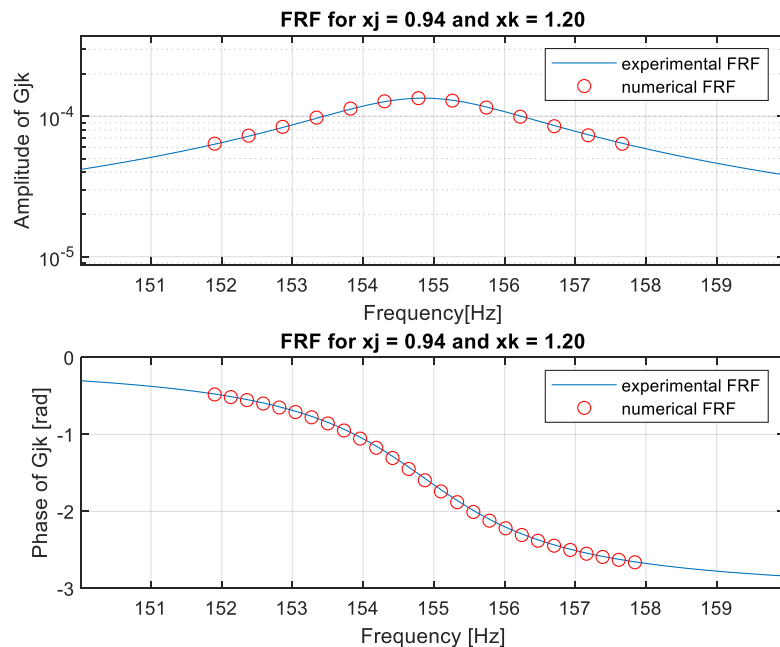


Figure 20: Fourth mode  $X_j=0.94$

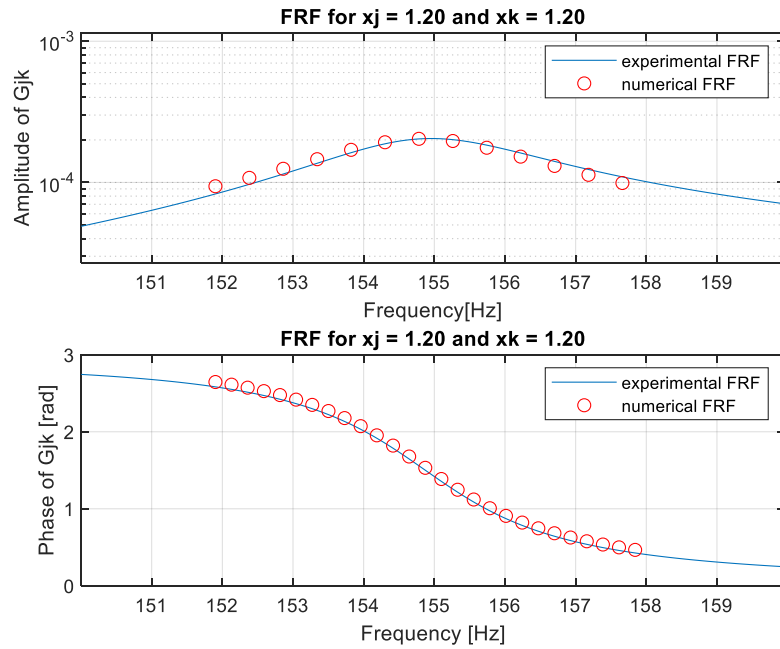


Figure 21: Fourth mode  $X_j=1.20$

#### *Overall quality check*

Figure 22, 23, 24 show the comparison between the experimental FRFs and the computed FRFs considering the entire frequency range, to evaluate the overall behaviour of the functions.

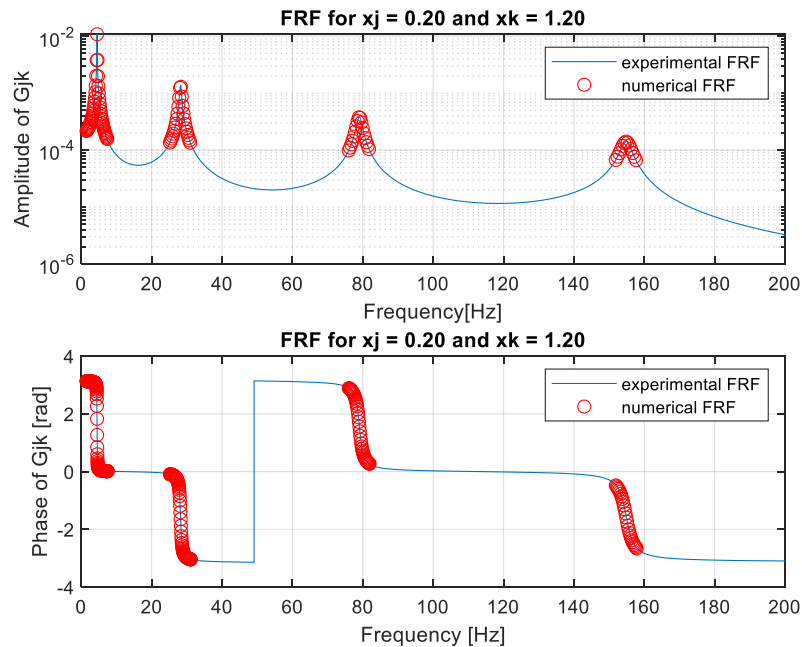


Figure 22:  $X_j=0.20$

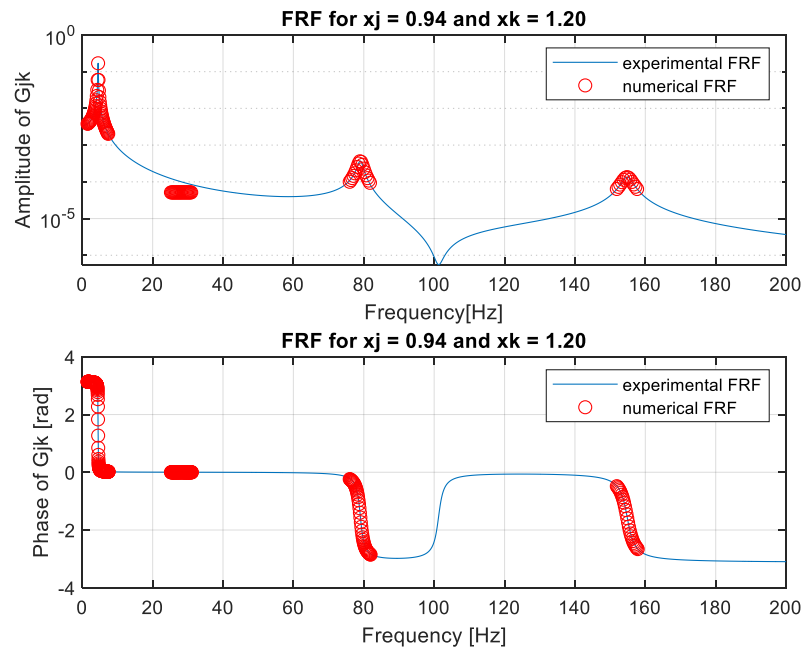


Figure 23:  $X_j=0.94$

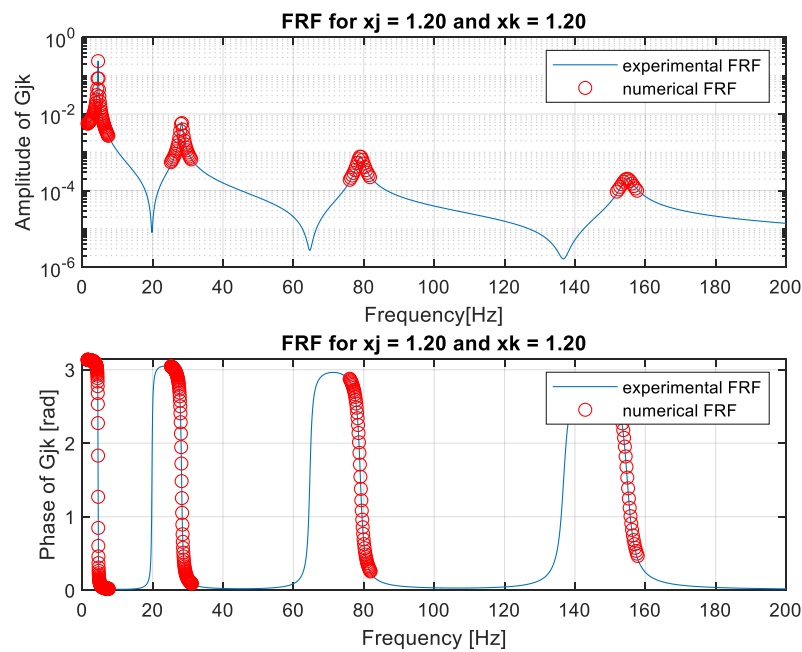


Figure 24:  $X_j=1.20$  Collocated FRF

## A.5. Identified parameters and mode shapes

The final item of part A of assignment 1 requires making a comparison between the identified parameters and the ones defined during the simulation stage. Furthermore, the identified mode shapes will be plotted onto the ones obtained in chapter A.1. shown in fig.4.

### Mode 1

The table below shows the results of the modal parameter identification of mode 1, in parameters terms. There is a very good agreement between both the natural frequencies (to the third decimal) and the damping ratios (to the third decimal).

	Natural frequency [Hz]	Damping ratio [%]
Model	4.504	1.000
Identified	4.504	1.000

Fig.25 shows the quality of the identification in terms of identified mode shape, by imposing the identified discrete modal vector values (dots) onto the continuous mode shape computed in A.1. A perfect alignment is shown. Notice that a common scaling factor equal to the maximum value of the identified mode shape has been applied.

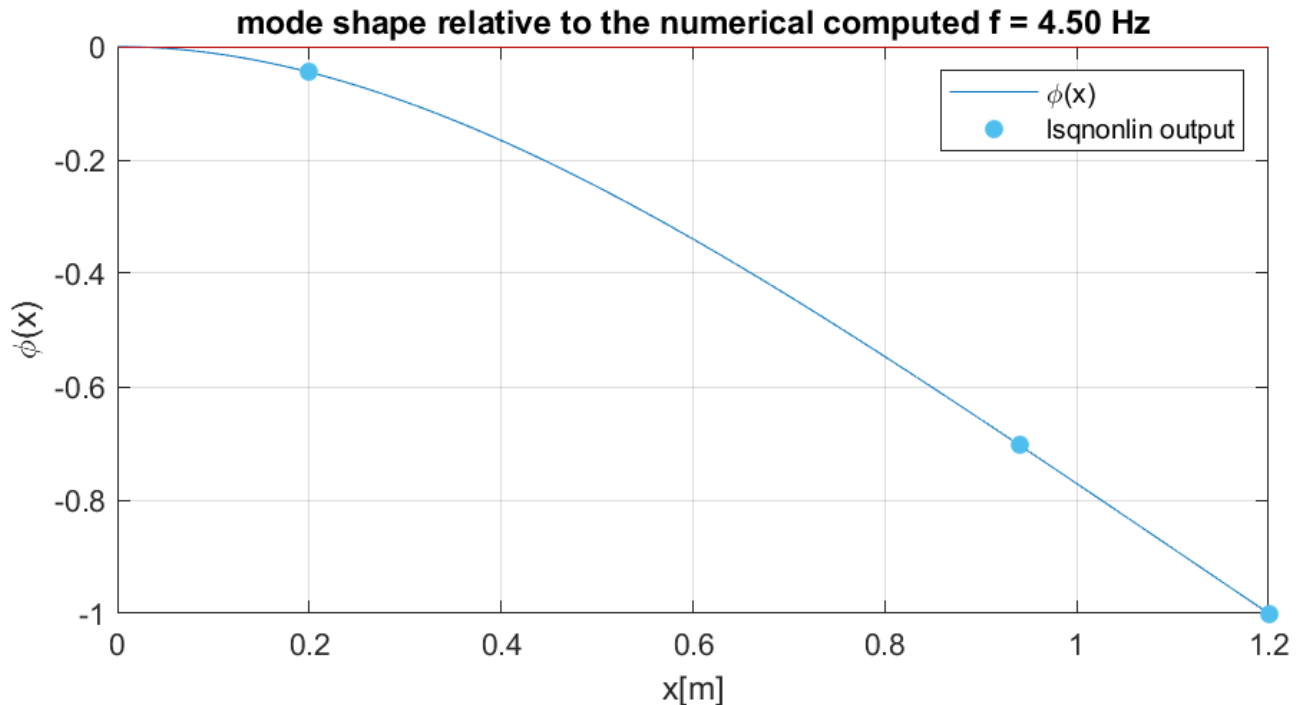


Figure25: Identified mode shape 1

### Mode 2

The table below shows the results of the modal parameter identification of mode 2, in parameters terms. There is a very good agreement between both the natural frequencies (to the second decimal) and the damping ratios (to the unit).

	Natural frequency [Hz]	Damping ratio [%]
Model	28.225	1.000
Identified	28.222	1.000

Fig.26 shows the quality of the identification in terms of identified mode shape, by imposing the identified discrete modal vector values (dots) onto the continuous mode shape computed in A.1. A perfect alignment is shown. Notice that a common scaling factor equal to the maximum value of the identified mode shape has been applied.

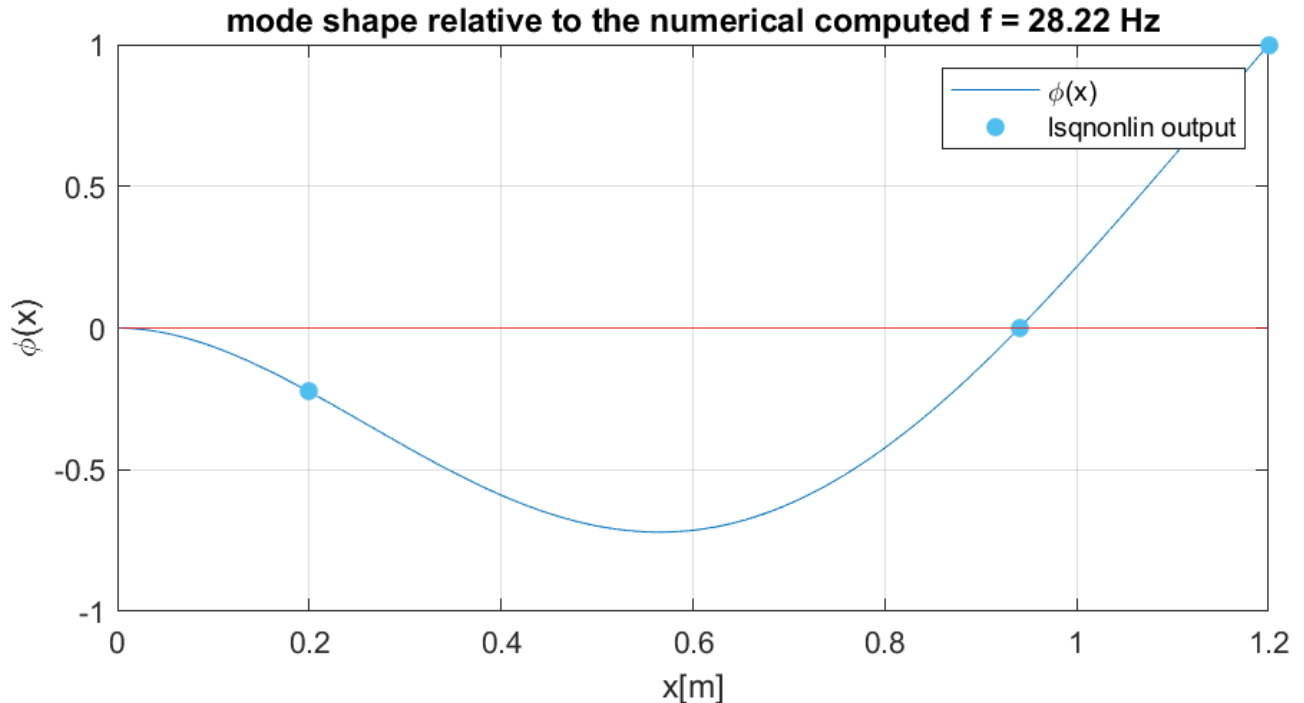


Figure 26: Identified mode shape 2

### Mode 3

The table in the next page shows the results of the modal parameter identification of mode 3, in parameters terms. There is a very good agreement between both the natural frequency (to the first decimal) and the damping ratio (to the unit).

	Natural frequency [Hz]	Damping ratio [%]
Model	79.031	1.000
Identified	79.024	1.000

Fig.27 shows the quality of the identification in terms of identified mode shape, by imposing the identified discrete modal vector values (dots) onto the continuous mode shape computed in A.1. A perfect alignment is shown. Notice that a common scaling factor equal to the maximum value of the identified mode shape has been applied.

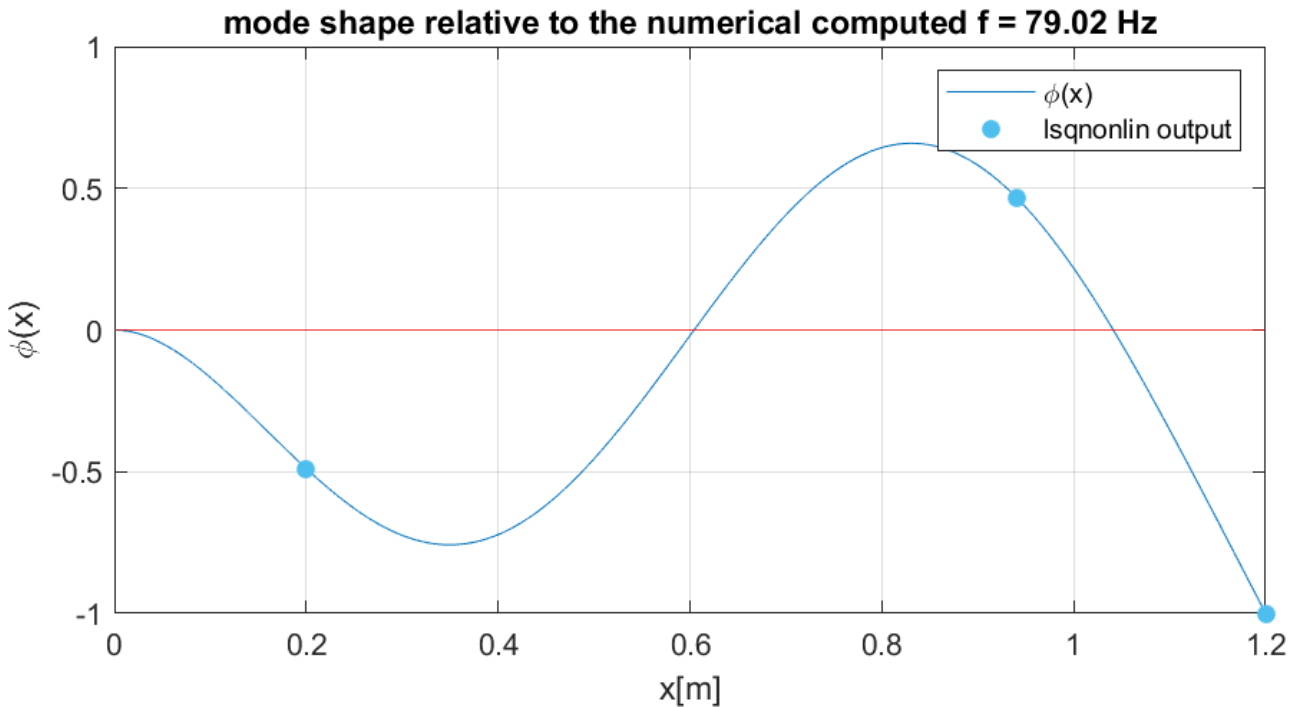


*Figure 27: Identified mode shape 3*

#### Mode 4

The table below shows the results of the modal parameter identification of mode 4, in parameters terms. There is a very good agreement between both the natural frequency (to the first decimal) and the damping ratio (to the unit).

	Natural frequency [Hz]	Damping ratio [%]
Model	154.868	1.000
Identified	154.832	1.000

Fig.28 shows the quality of the identification in terms of identified mode shape, by imposing the identified discrete modal vector values (dots) onto the continuous mode shape computed in A.1. A perfect alignment is shown. Notice that a common scaling factor equal to the maximum value of the identified mode shape has been applied.

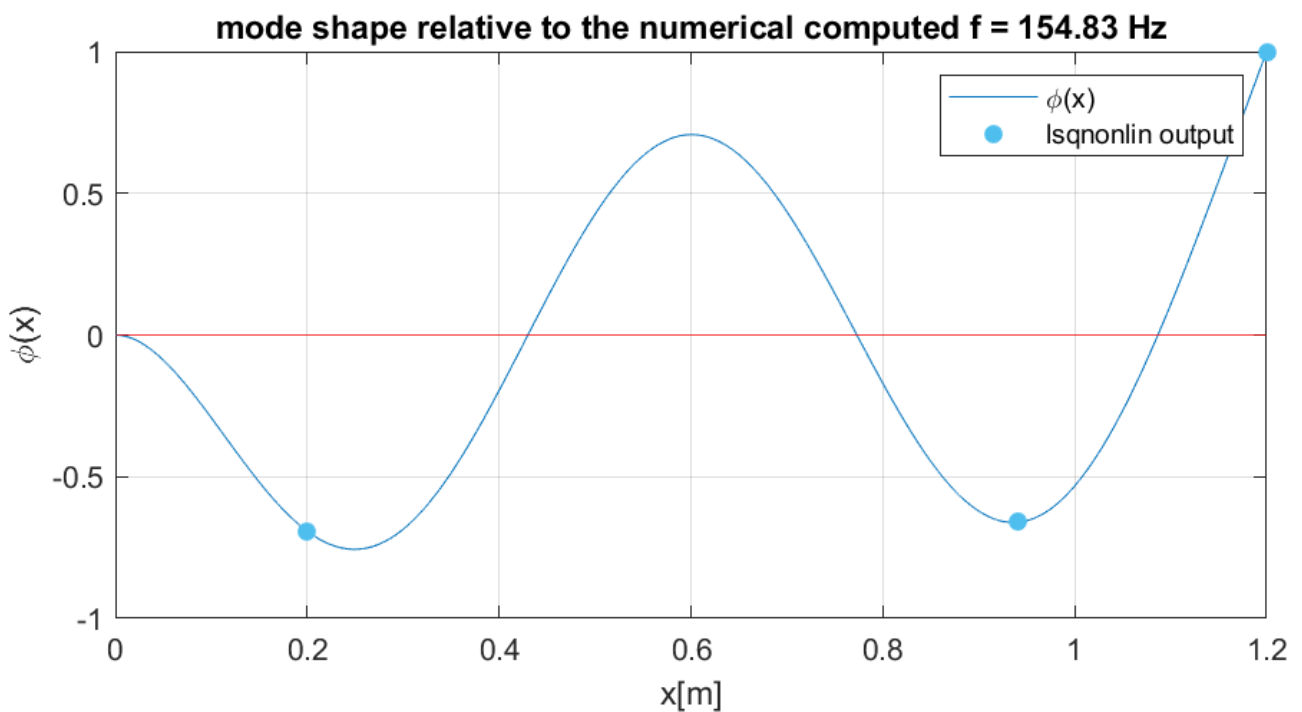


Figure 28: Identified mode shape 4

## Part B: Experimental Modal Analysis of a light rail wheel

### Introduction

The aim of this second part of the assignment is to implement a numerical procedure to identify the natural frequencies, the corresponding mode shapes and the damping ratio of a resilient light rail wheel starting from a set of experimental data. The computation of the modal parameters has been performed by applying an FRF multi-mode curve fitting method, that consists in numerically identifying the set of parameters that corresponds to the most accurate approximation of the given inertance FRFs.

During the measurement campaign, the resilient wheel was suspended through elastic supports (free-free system) disposed in a non-symmetric configuration (this has an impact on the result); the input was provided through a dynamometric hammer in terms of an axial impulsive load, while the output was measured in terms of acceleration. For this purpose, 12 accelerometers were placed on the wheel rim to sense the axial vibration; they were all located on the same half on the wheel and positioned 15° apart from each other covering an angle between 0° and 165° (axis symmetry of the system was exploited). Note that the input force was applied opposite to the first accelerometer (angular position 180°), therefore collocated frequency response functions haven't been considered.

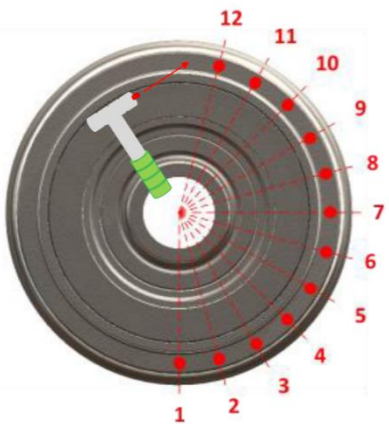


Figure 29: position of the accelerometers



Figure 30: resilient wheel

The first section of this assignment is going to present a brief overview of the experimental inertance FRFs provided and of the procedure that has been followed to identify the modal parameters; then, the quality of the results is going to be evaluated through a direct comparison between the plot of the numerical result and the original data. In the end, the natural frequencies and the corresponding mode shapes are also going to be discussed.

## B.1. Modal parameter identification

The given data consists in:

- a set of twelve inertance FRFs, that illustrate the response of the system when subject to axial load
- a frequency vector that indicates the frequency range of interest (between 0 and 5000 Hz)
- a set of twelve coherence functions, that provide information about the correlation between the input and the output (if correlation is low, it means that the measured acceleration is not associated to the axial load)

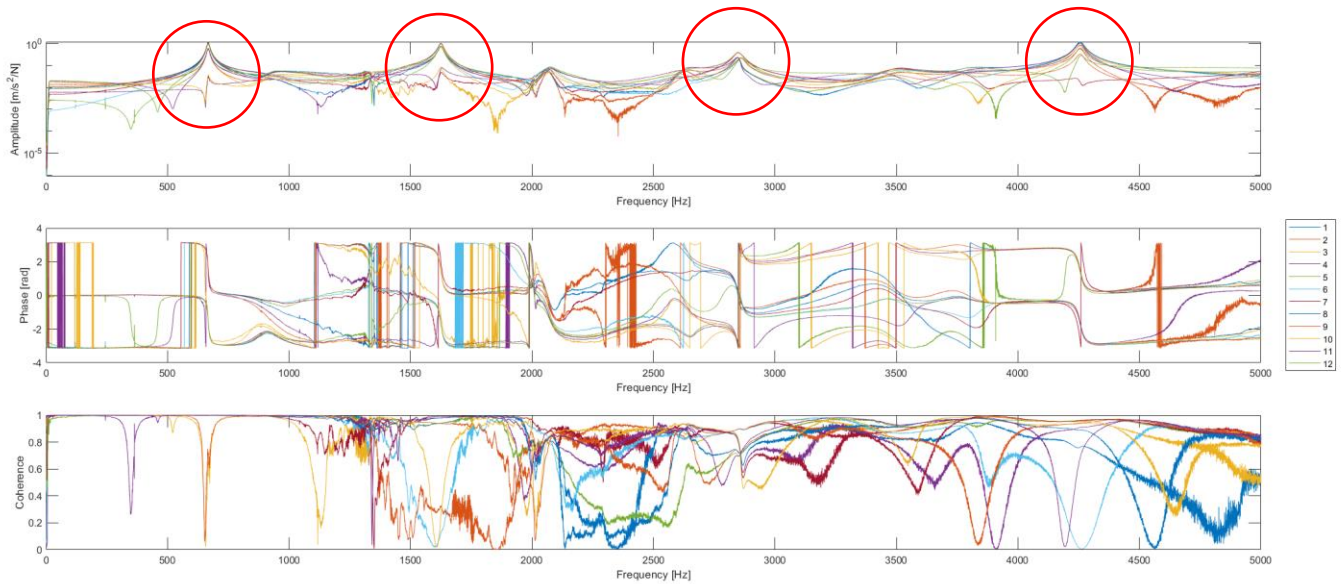


Figure 31: inertance FRFs given as unput

Some preliminary observations can be performed:

- 4 main peaks can be identified: they are the ones associated to the axial natural frequencies that have been excited (circled in red). The other peaks instead are associated to the radial natural frequencies; their presence in the FRFs associated to the axial vibration suggests a coupling between the axial input and the radial vibration of the wheel
- low coherence is observed at high frequency, it is associated to the reduced capability of exciting those natural frequencies during the experiment (the bigger the hammer, the lower the frequency range, the harder the tip, the higher the frequency range)

- Peak 1:

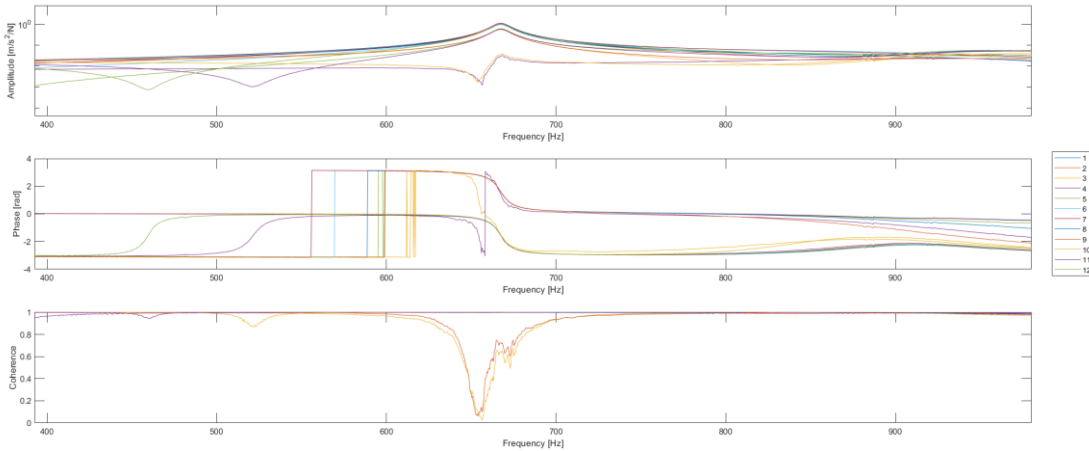


Figure 32: first peak

- All the FRFs have a single resonance peak in correspondence of the same frequency except for the ones associated to accelerometers 4 and 10, that have a significantly different shape
- This behavior is related to the fact that those two accelerometers are very close to a node, in a position such that the pole-zero cancellation is not perfect; for this reason, the curves have the typical behavior of an antiresonance (zero of the FRF) and immediately after of a resonance (pole of the FRF)
- The vicinity of a vibration node also explains the remarkable drop in the coherence, and it can be associated to a low signal to noise ratio (the accelerometer is measuring noise not vibration)

- Peak 2:

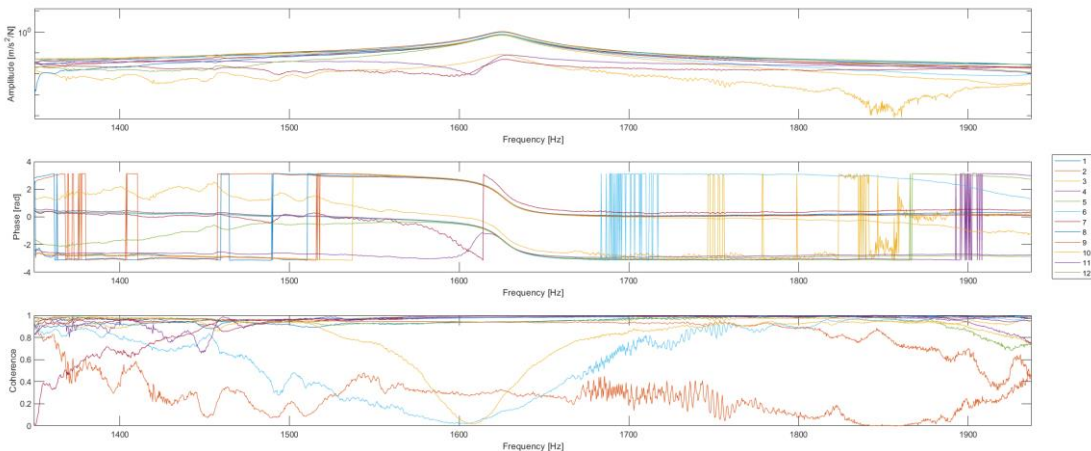


Figure 33: second peak

- Similarly to Peak 1, all FRFs have a single peak except the ones associated to accelerometers 11 and 7, that have a significantly different shape
- This behavior is once again related to a non-perfect pole-zero cancellation

- Peak 3:

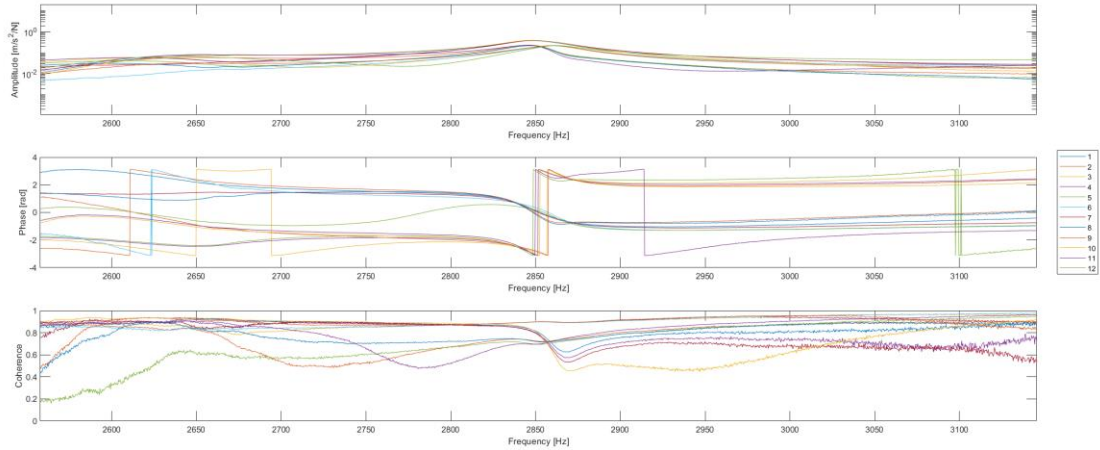


Figure 34: third peak

- Two peaks can be seen 20 Hz apart from each other, and this difference is large enough to consider them two different and separate natural frequencies (associated to two different vibration modes)
- Note that none of the FRFs show both peaks: some have a resonance at a frequency  $f_3$  (associated to accelerometers 1,2,4,5,7,8,10,11), others at  $f_3 + 20 \text{ Hz}$  (associated to accelerometers 3,6,9,12)
- This phenomenon is related to the fact that the assumption of axis symmetry is incorrect: the asymmetric distribution of the springs that keep the resilient wheel suspended locally modifies the stiffness of the system. As a matter of fact, not all the sectors covered by the 12 accelerometers are affected in the same way by the presence of the springs
- Increasing the number of springs would have been a better choice to make sure every section had the same properties in terms of stiffness
- This effect could potentially be observed in every peak but if the wavelength is high enough (if the frequency is low enough), then it is not present (as in this case)
- The two vibration modes associated to the two natural frequencies have the same shape and number of nodal diameters, but are rotated one with respect to the other

- Peak 4

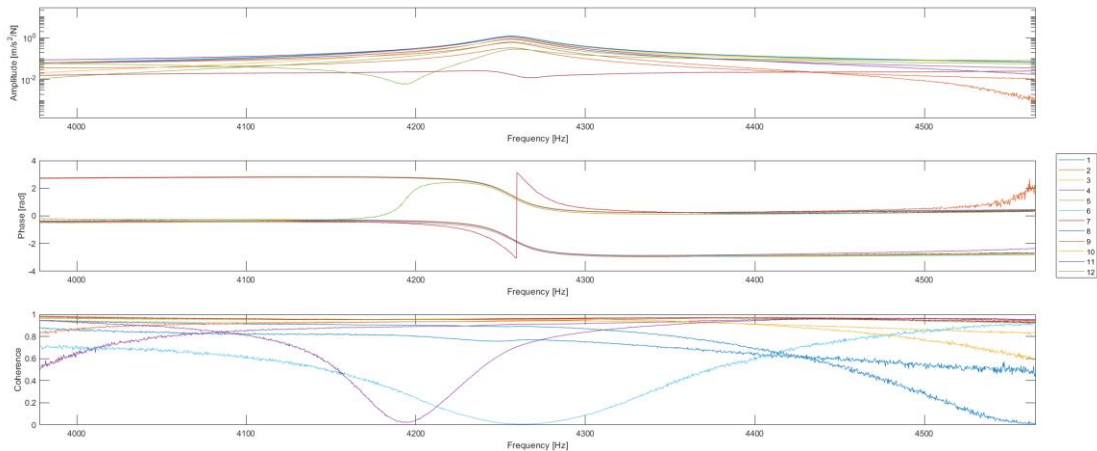


Figure 35: fourth peak

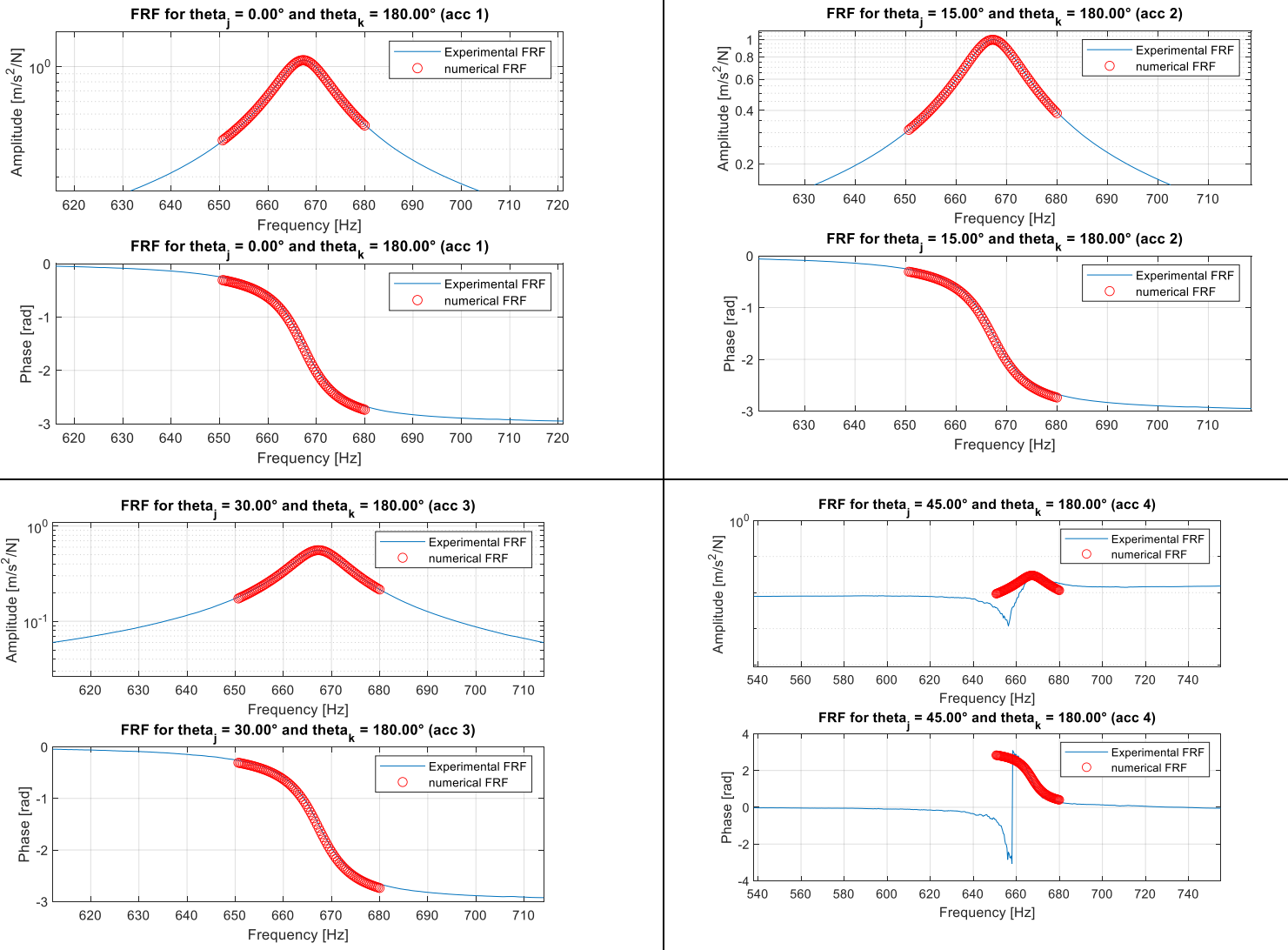
- Similarly to Peak 1, all FRFs have a single peak except the ones associated to accelerometers 7 and 12, that have a significantly different shape
- This behavior is once again related to a non-perfect pole-zero cancellation (for accelerometer 7 the curve is almost flat, this means it is located extremely close to a node for that vibration mode)

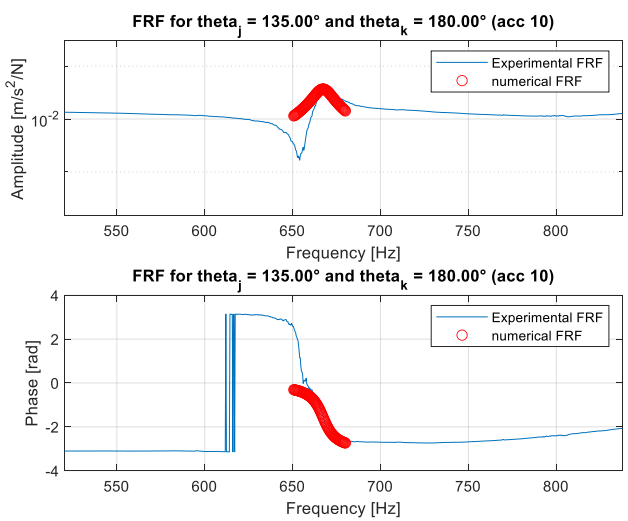
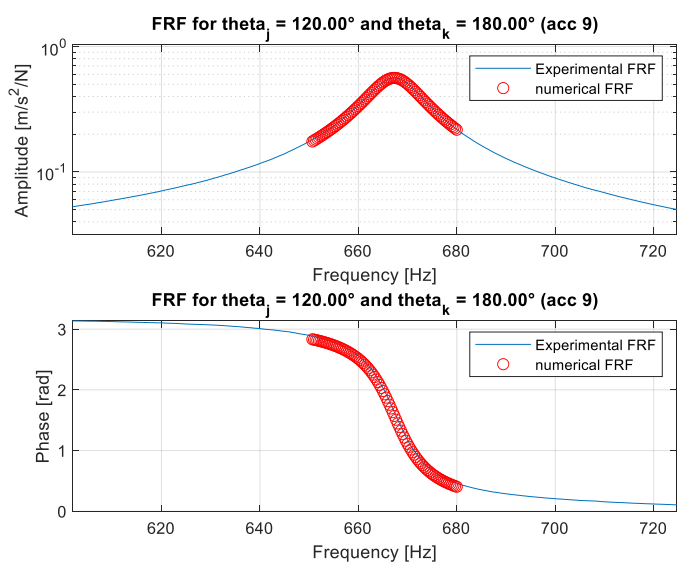
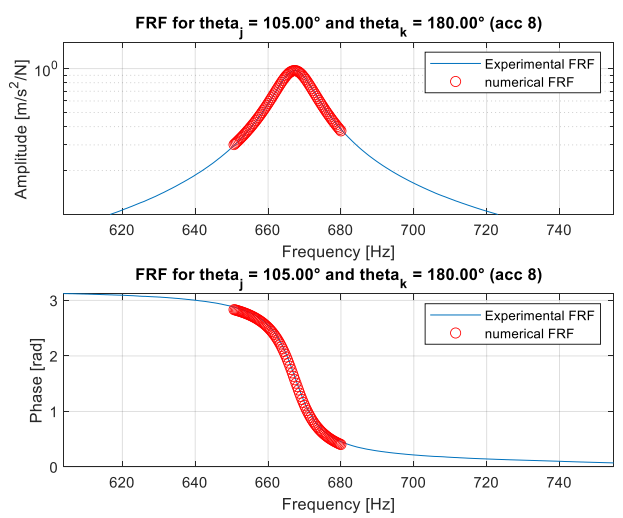
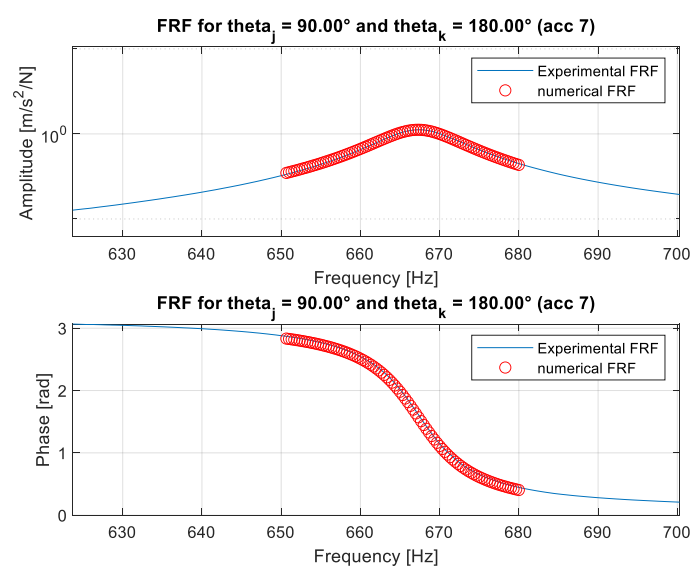
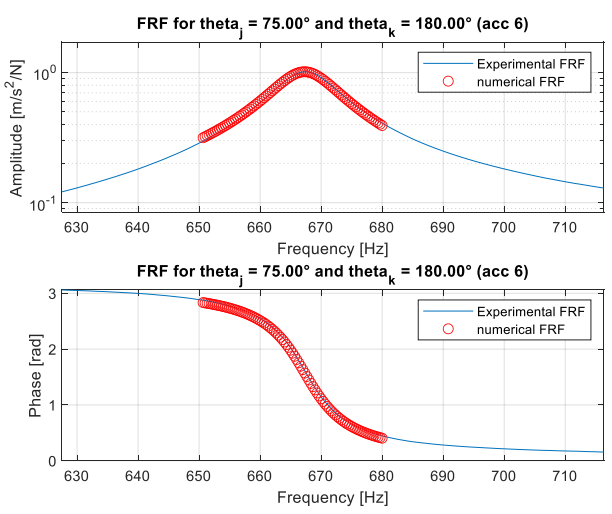
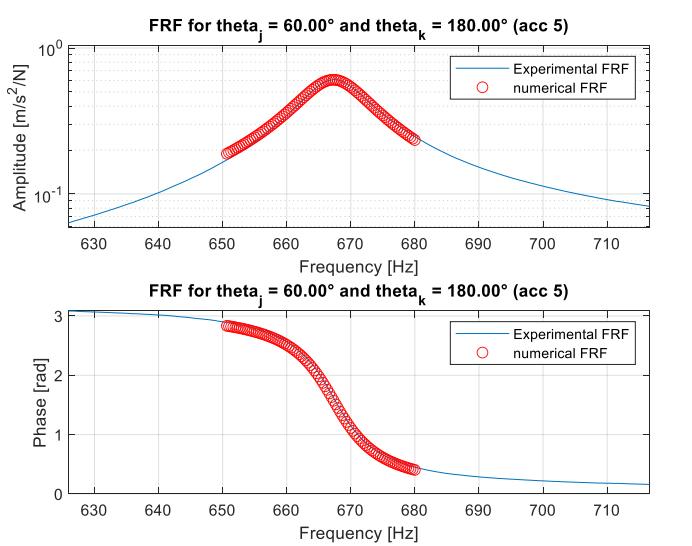
The procedure followed to compute the modal parameters is the same one applied in section A3. Note that the blue line represents the experimental FRFs while the circles represent the numerical approximation.

## B.2. Quality of the identification

### Mode 1 quality check

The numerical results are consistent with the observations made in the previous chapter: in every FRF the first peak is reconstructed with good precision except for the ones associated with accelerometers 4 and 10. In the following table, the numerical approximation of the first peak in every FRF is displayed. Note that  $\theta_j$  is the position where the input force was applied and  $\theta_k$  is the position where the acceleration was measured.





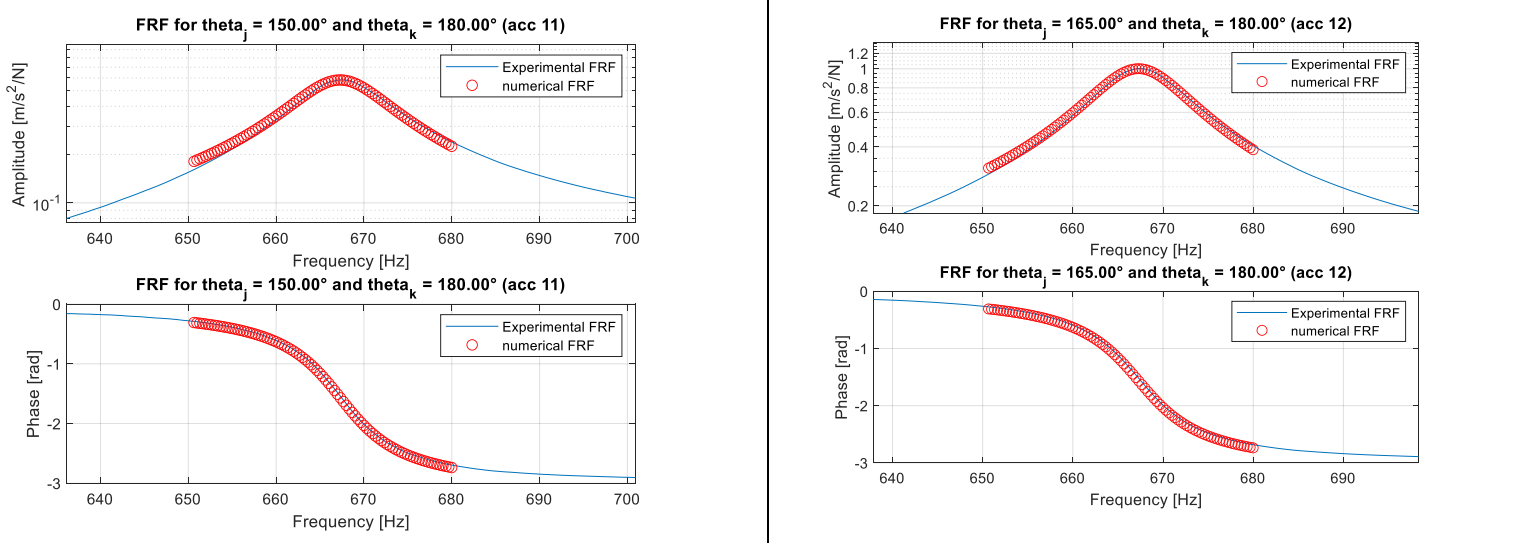
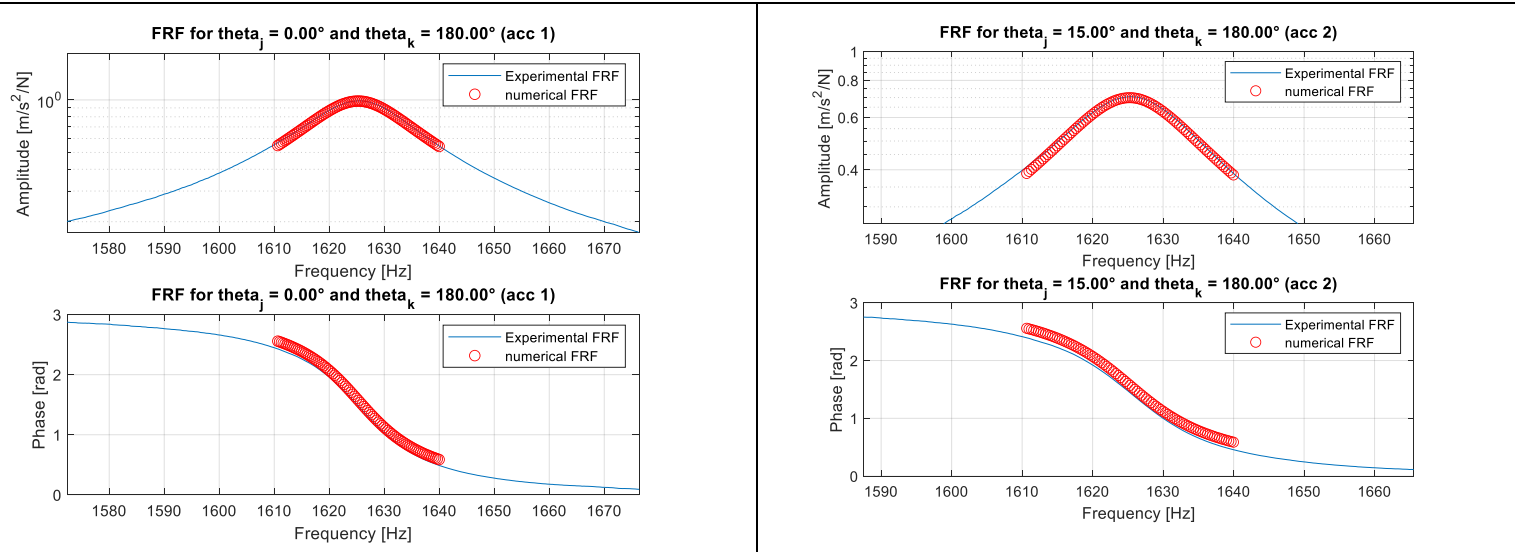
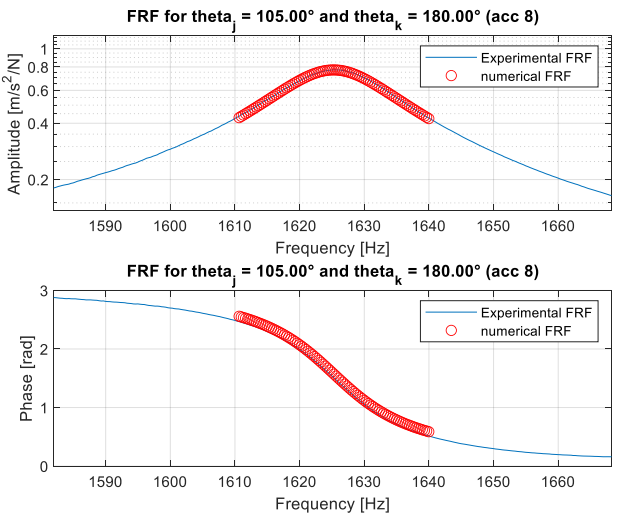
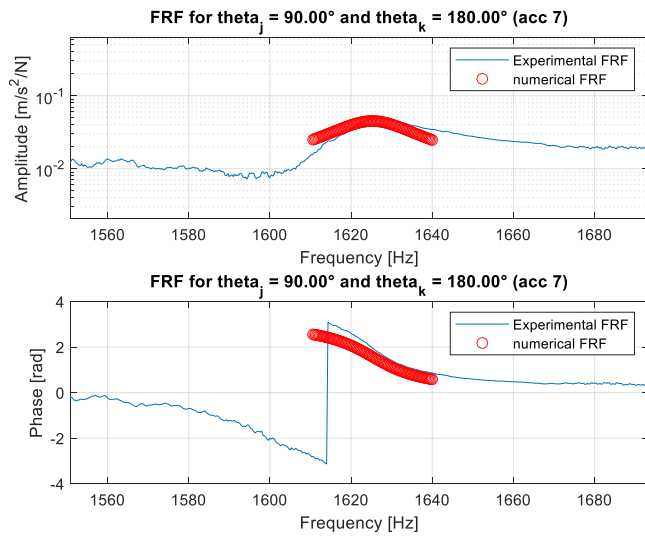
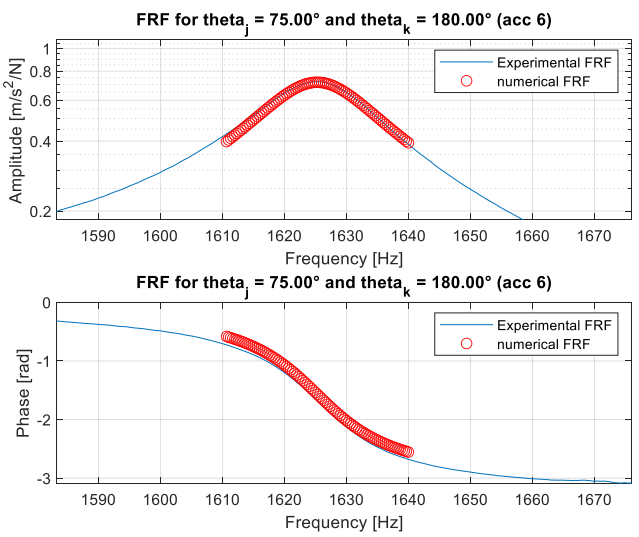
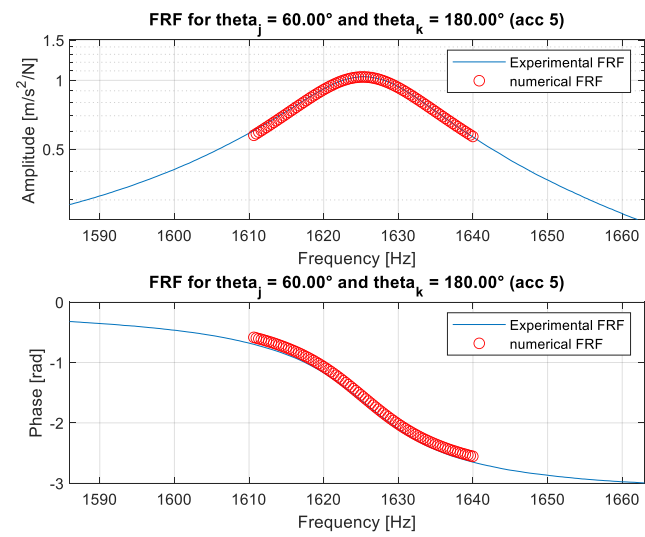
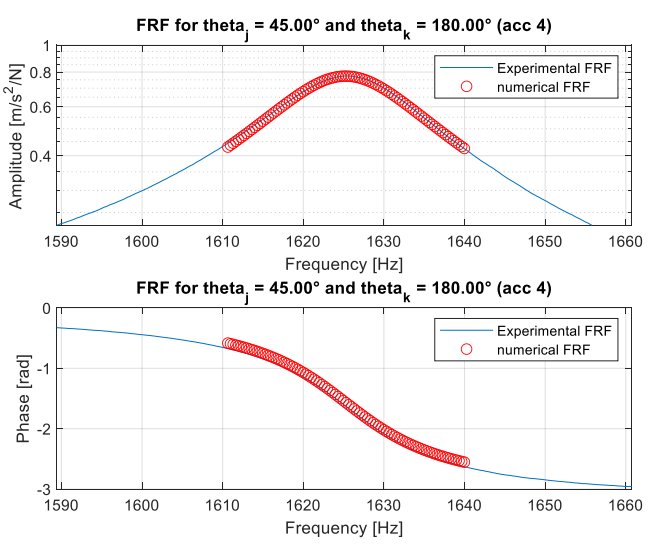
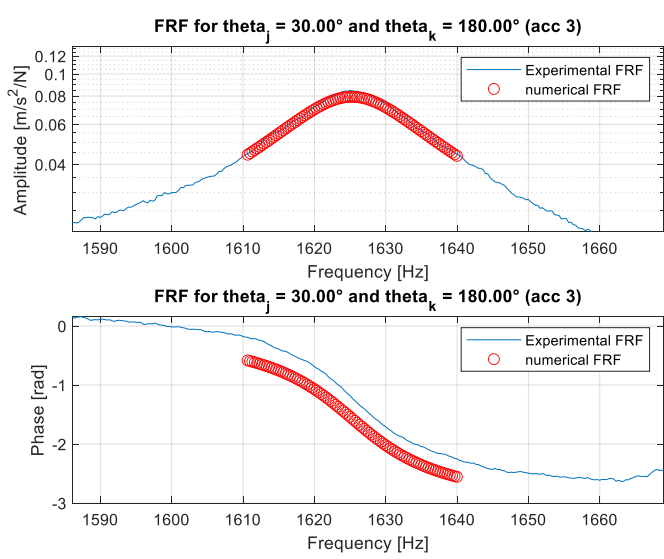


Table 1: numerical identification of the first vibration mode

### Mode 2 quality check

The numerical results are consistent with the observations made in the previous chapter: in every FRF the first peak is reconstructed with good precision except for the ones associated with accelerometers 7 and 11. In the following table, the numerical approximation of the second peak in every FRF is displayed. Note that  $\theta_k$  is the position where the input force was applied and  $\theta_j$  is the position where the acceleration was measured.





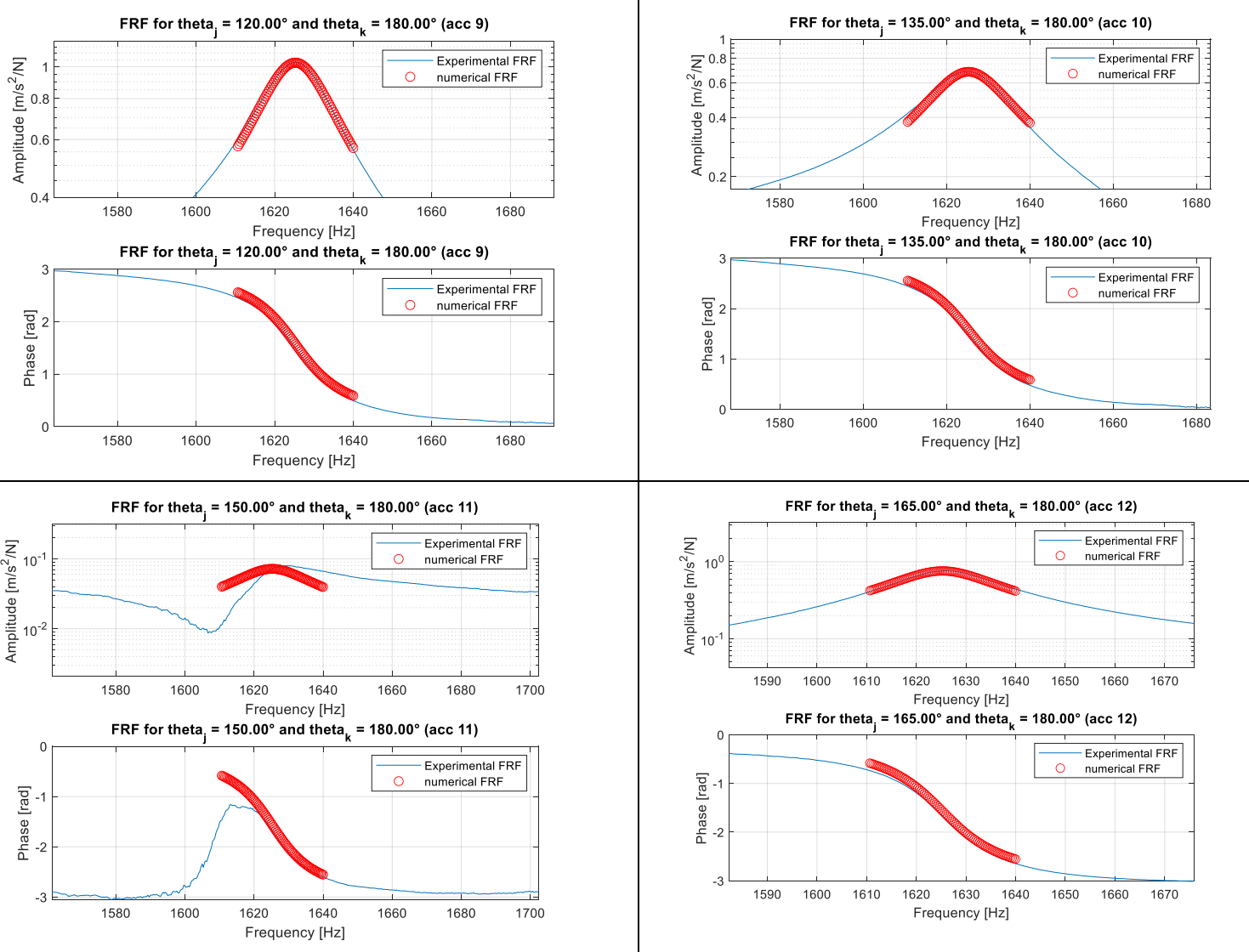


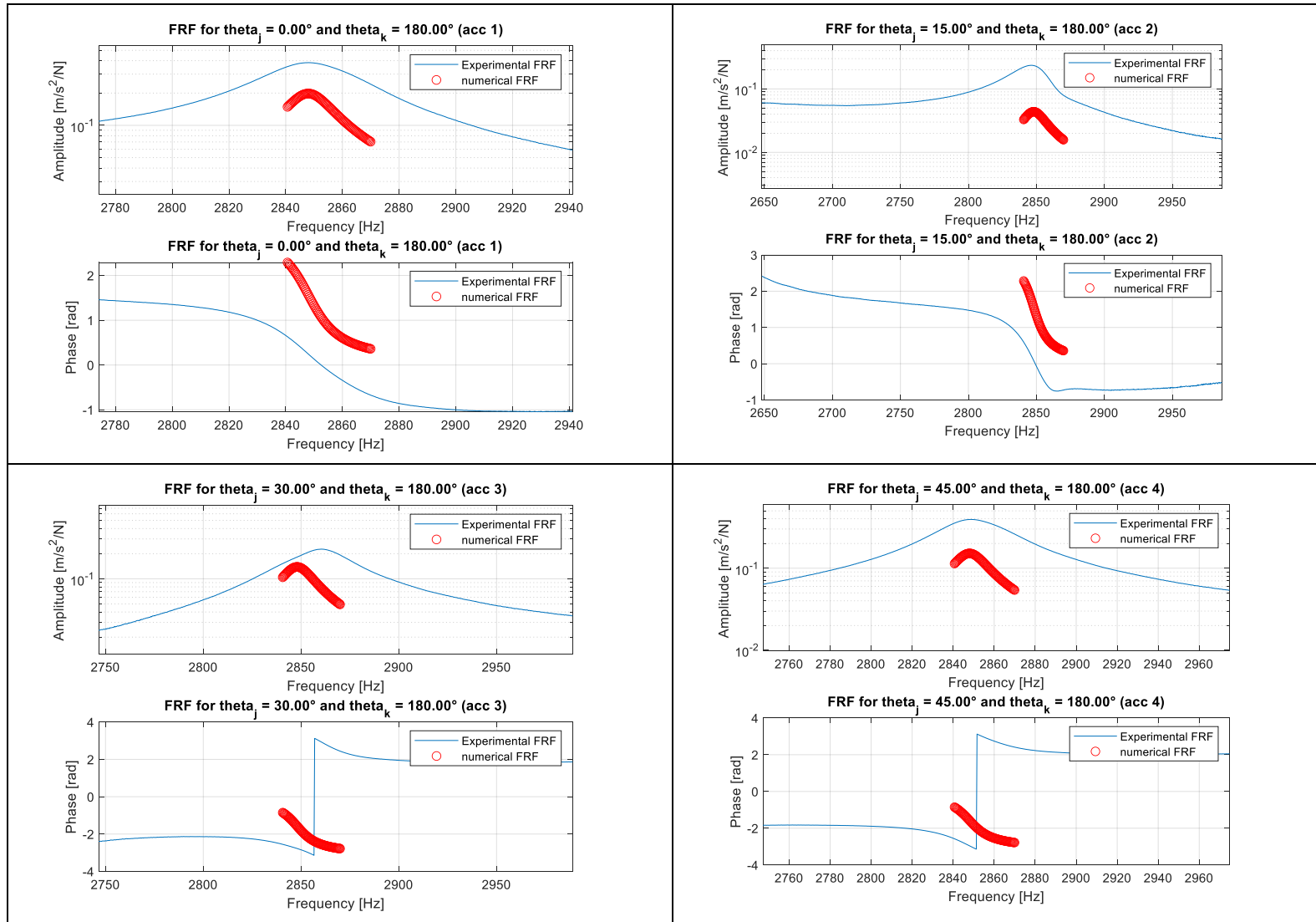
Table 2: numerical identification of the second vibration mode

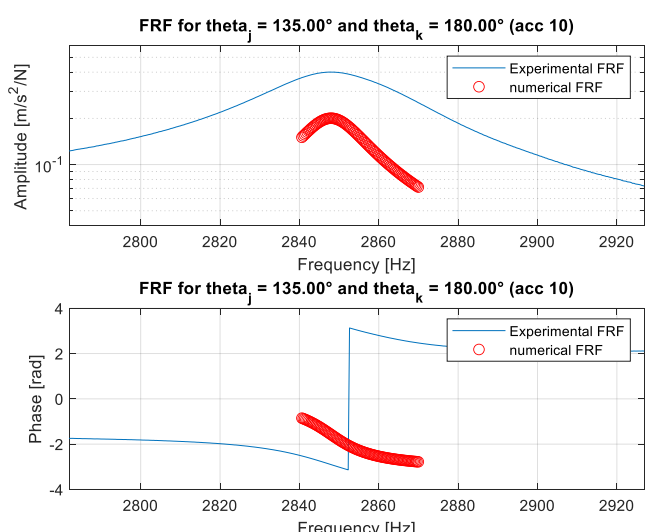
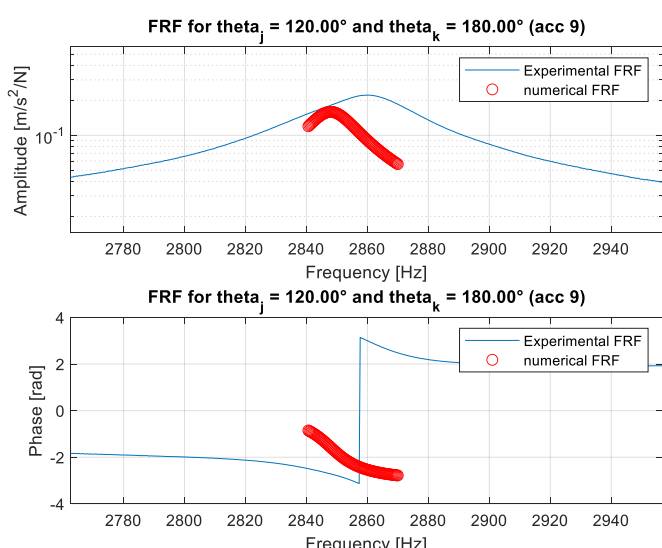
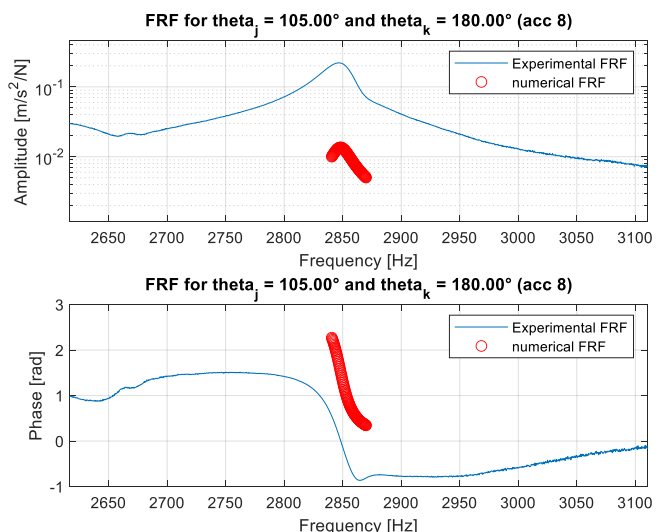
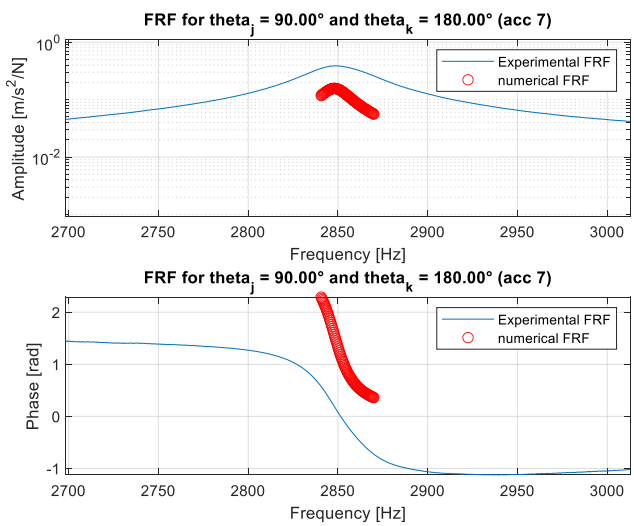
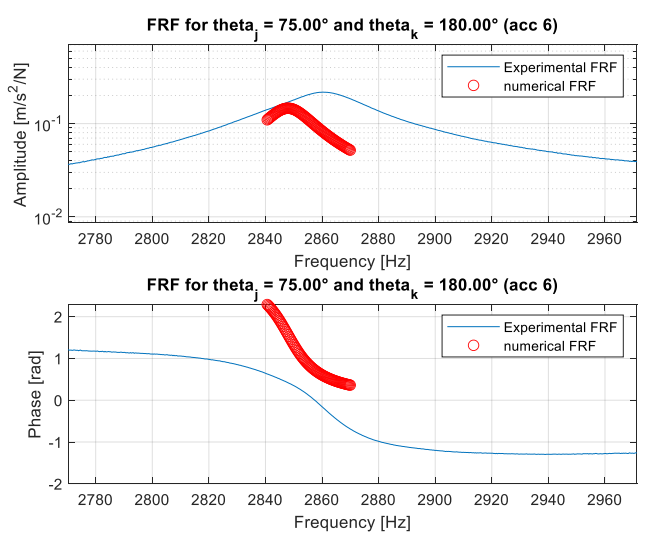
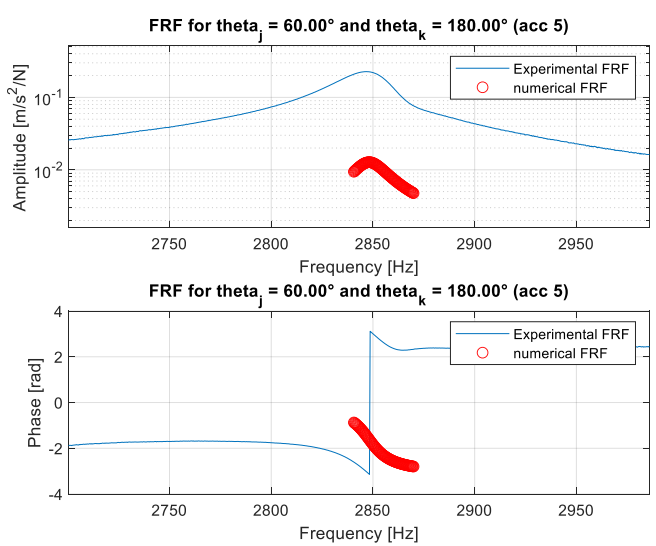
### Mode 3 quality check

In this case, the quality of the numerical results is extremely poor: in every FRF neither of the two peaks has been identified correctly, either in terms of natural frequency or in terms of damping. To account for this problem, a couple of different solutions can be considered

- Implementing a full multi-mode curve fitting method that can identify more than one peak for each frequency range considered
- Reduce the frequency range considered to include only one of the two peaks at a time (still performing the minimization considering all the set of FRFs)
- Perform two different minimizations, considering for each peak only the FRFs that show that specific resonance (in this case, one option could be to perform a minimization considering FRFs number 1,2,4,5,7,8,10,11 to characterize the first peak and another one considering FRFs number 3,6,9,12 to characterize the second one)

In the following table, the numerical approximation of the third peak in every FRF is displayed. Note that  $\theta_k$  is the position where the input force was applied and  $\theta_j$  is the position where the acceleration was measured.





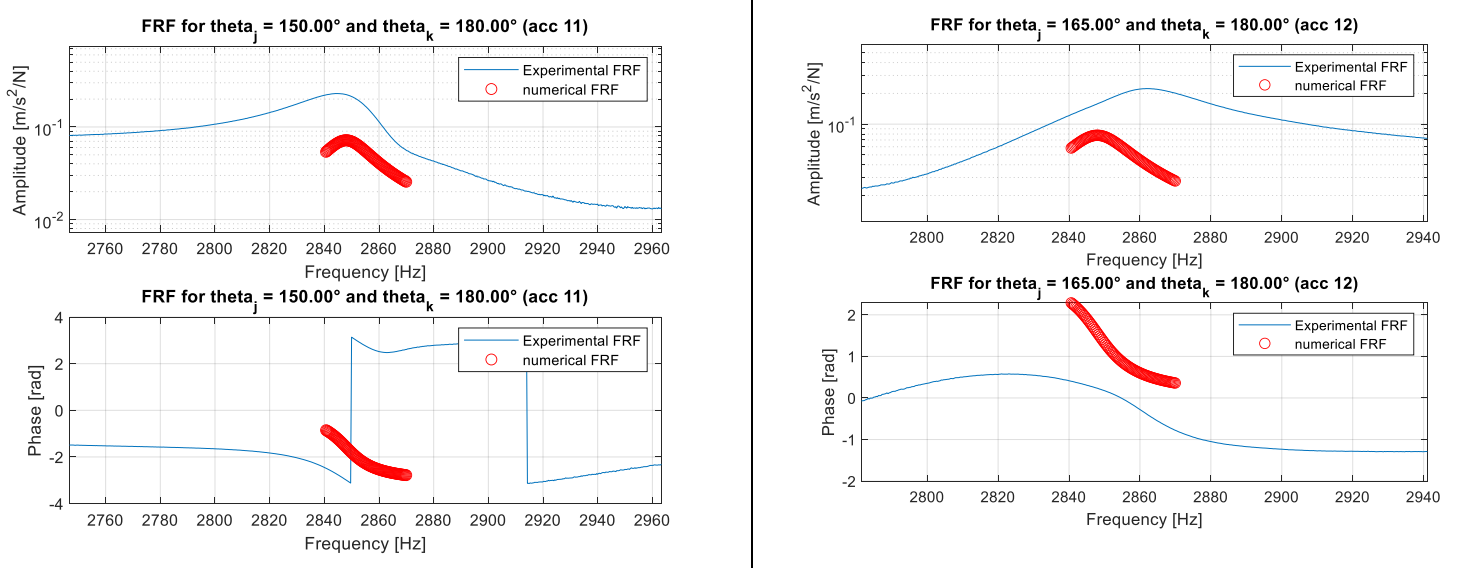
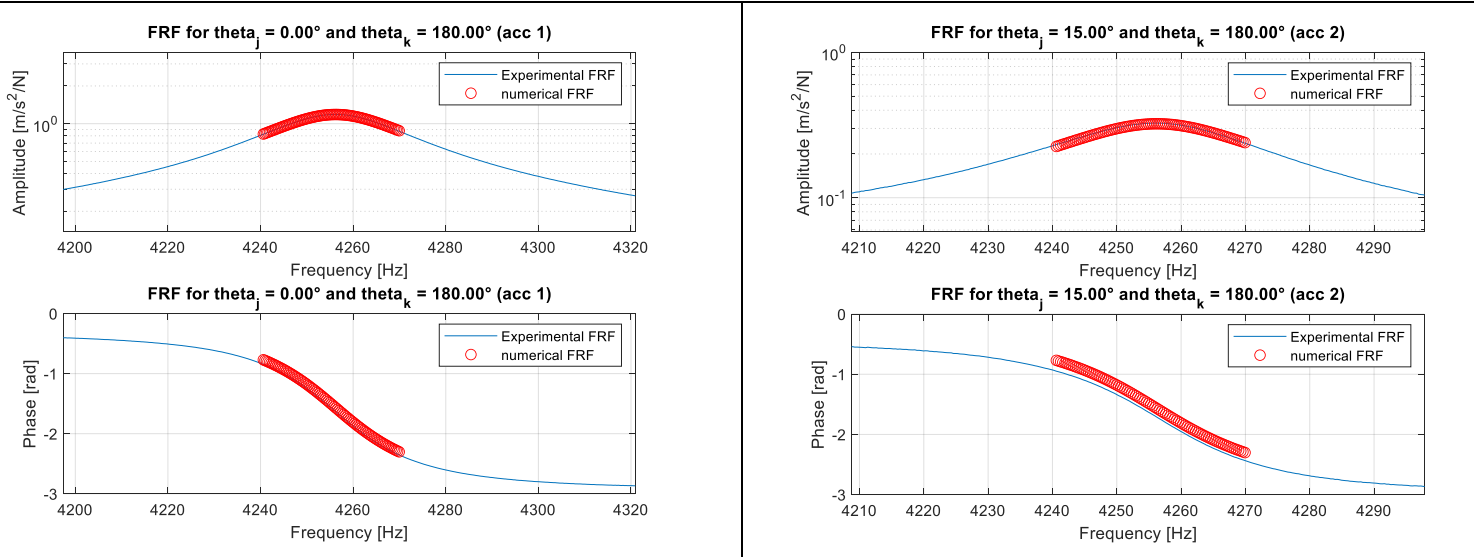
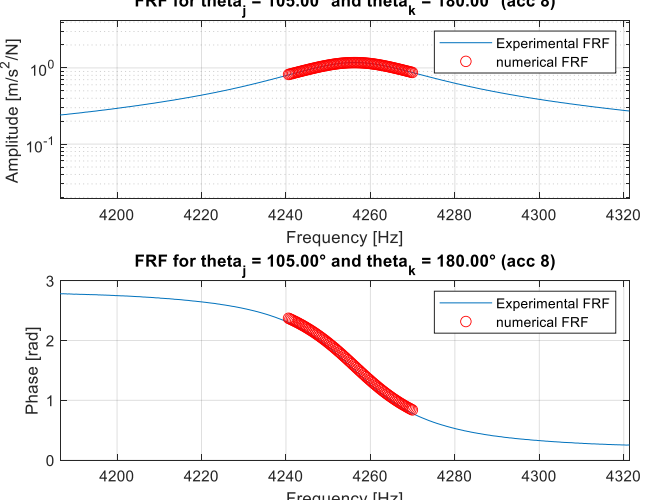
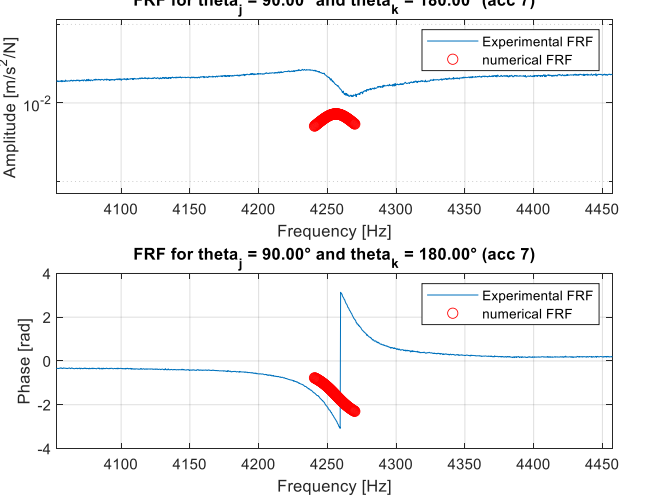
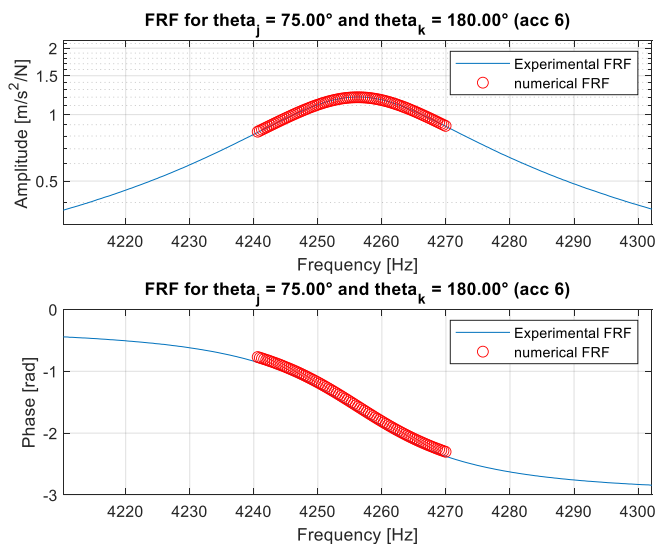
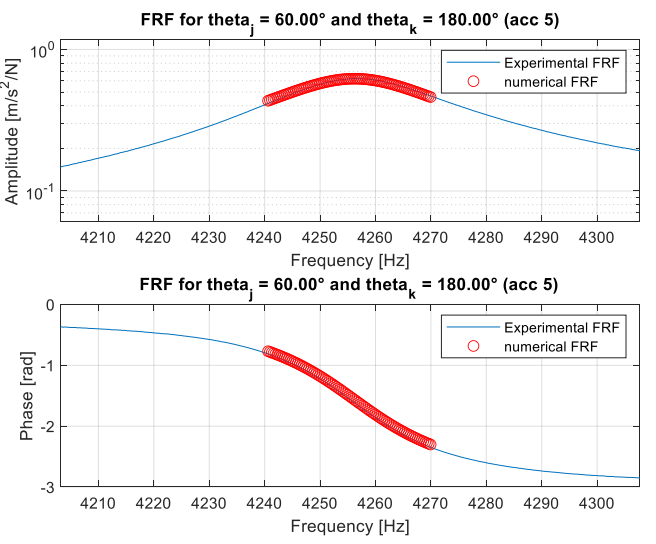
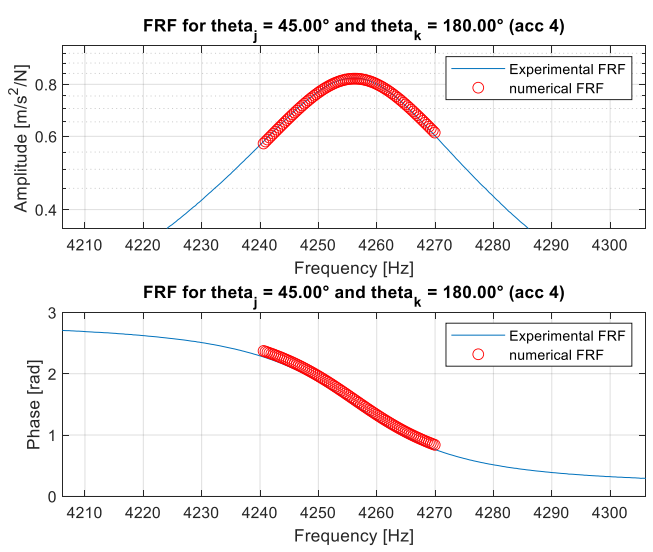
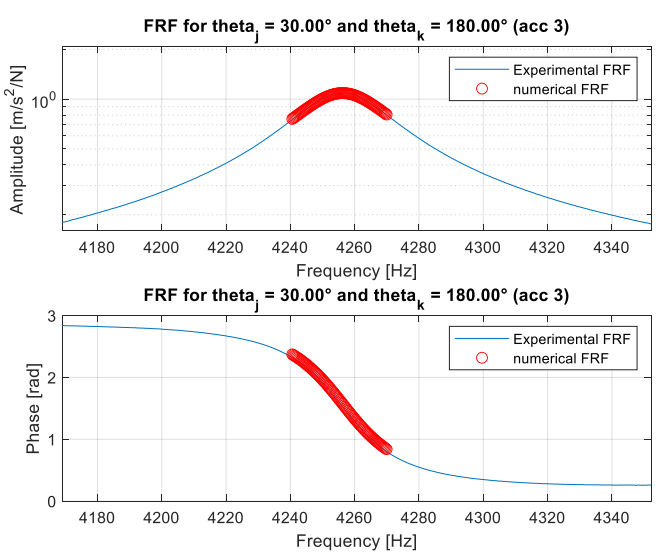


Table 3: numerical identification of the third vibration mode

#### Mode 4 quality check

The numerical results are consistent with the observations made in the previous chapter: in every FRF the first peak is reconstructed with good precision except for the ones associated with accelerometers 7 and 12. In the following table, the numerical approximation of the first peak in every FRF is displayed. Note that  $\theta_k$  is the position where the input force was applied and  $\theta_j$  is the position where the acceleration was measured.





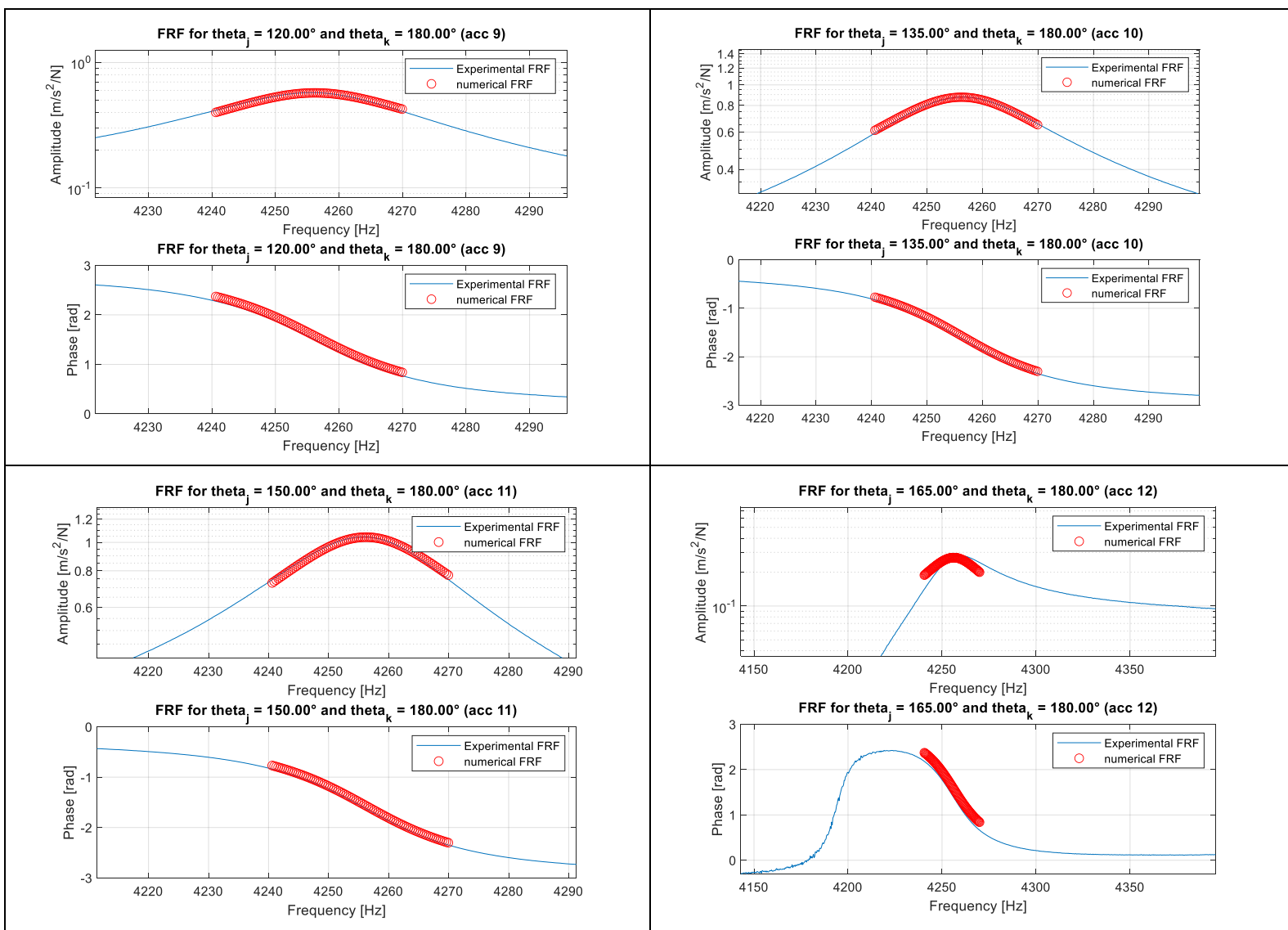


Table 4: numerical identification of the fourth vibration mode

### B.3. Identified parameters and mode shapes

#### Mode 1

The numerical approximation of the first mode has provided the following results:

Natural frequency [Hz]	Damping ratio [%]
667.324	0.805

In Fig.36 the mode shape associated with the first vibration mode is displayed. The dashed line represents the undeformed shape of the wheel, and the blue dots represent the results of the numerical minimization. The procedure described in the previous chapters indeed, provides also the modal vector associated to the correspondent natural frequency (each element of the modal vector approximates the mode shape in the position of the accelerometer). In the end, the results have been normalized, mirrored and interpolated.

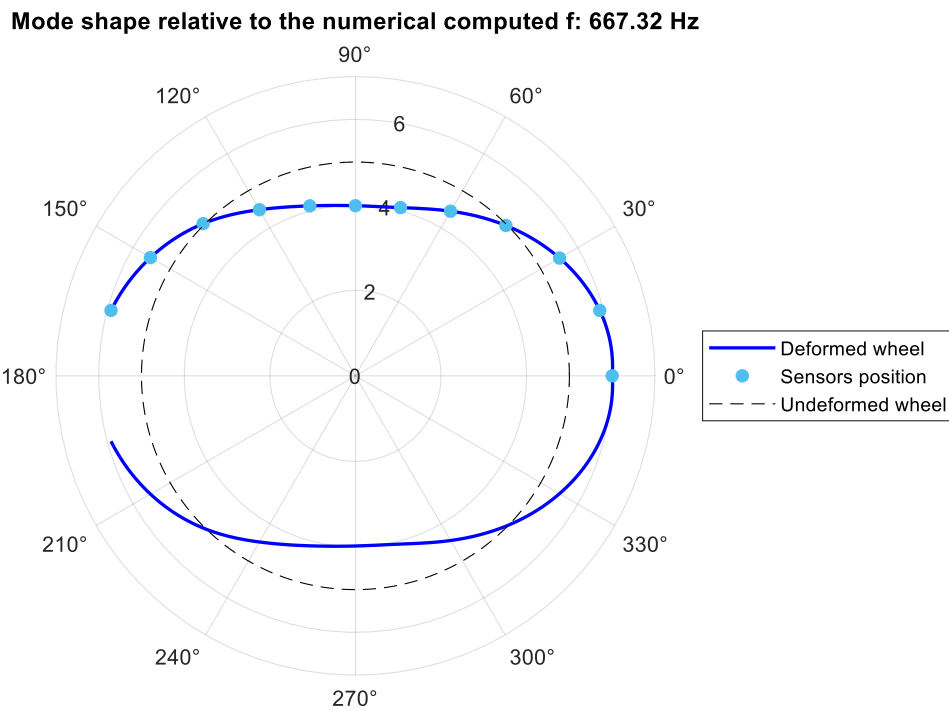


Figure 36: mode shape associated with the first natural frequency

## Mode 2

The numerical approximation of the first mode has provided the following results:

Natural frequency [Hz]	Damping ratio [%]
1625.312	0.598

In Fig.37 the mode shape associated with the second vibration mode is displayed. The dashed line represents the undeformed shape of the wheel, and the blue dots represent the results of the numerical minimization. The procedure described in the previous chapters indeed, provides also the modal vector associated to the correspondent natural frequency (each element of the modal vector approximates the mode shape in the position of the accelerometer). In the end, the results have been normalized, mirrored and interpolated.

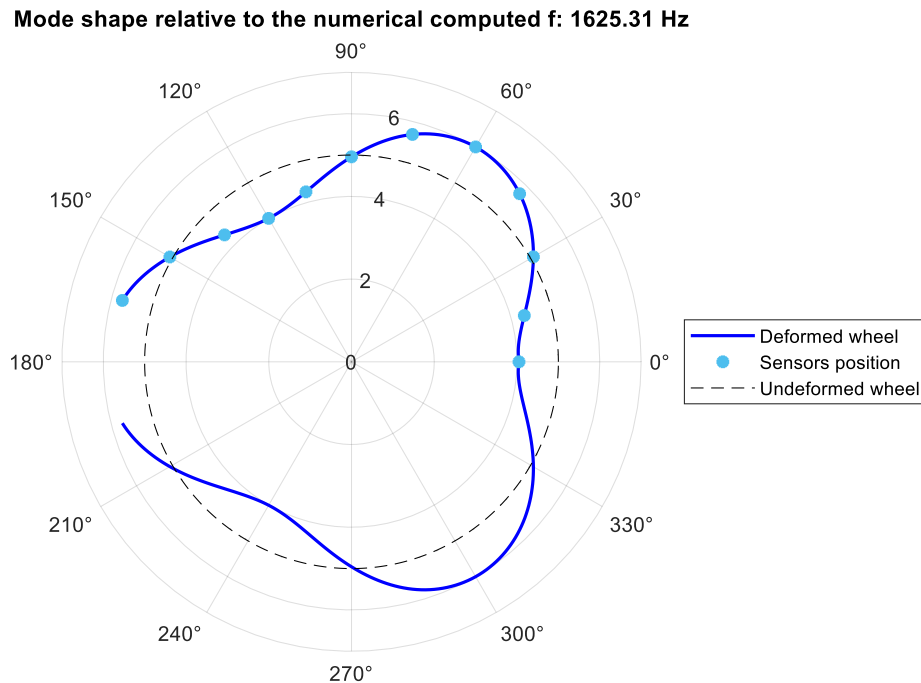


Figure 37: mode shape associated with the second natural frequency

### Mode 3

The numerical approximation of the first mode has provided the following results:

Natural frequency [Hz]	Damping ratio [%]
2847.962	0.293

In Fig.38 the mode shape associated with the fourth vibration mode is displayed. The dashed line represents the undeformed shape of the wheel and the blue dots represent the results of the numerical minimization. The procedure described in the previous chapters indeed, provides also the modal vector associated to the correspondent natural frequency (each element of the modal vector approximates the mode shape in the position of the accelerometer). In the end, the results have been normalized, mirrored and interpolated.

Since the results of the numerical approximation for the third peak were extremely poor, the modal parameters are just a rough approximation of the exact values, the mode shape has been computed anyways and the low quality of the results can be seen in the asymmetry of the mode shape.

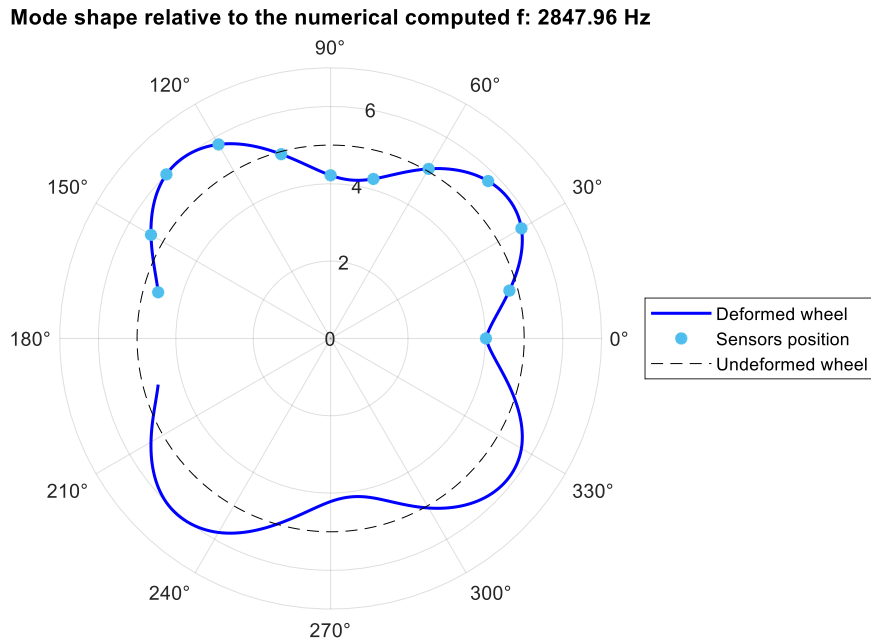


Figure 38: mode shape associated with the third natural frequency

#### Mode 4

The numerical approximation of the first mode has provided the following results:

Natural frequency [Hz]	Damping ratio [%]
4256.277	0.357

In Fig. 39 the mode shape associated with the fourth vibration mode is displayed. The dashed line represents the undeformed shape of the wheel and the blue dots represent the results of the numerical minimization. The procedure described in the previous chapters indeed, provides also the modal vector associated to the correspondent natural frequency (each element of the modal vector approximates the mode shape in the position of the accelerometer). In the end, the results have been normalized, mirrored and interpolated.

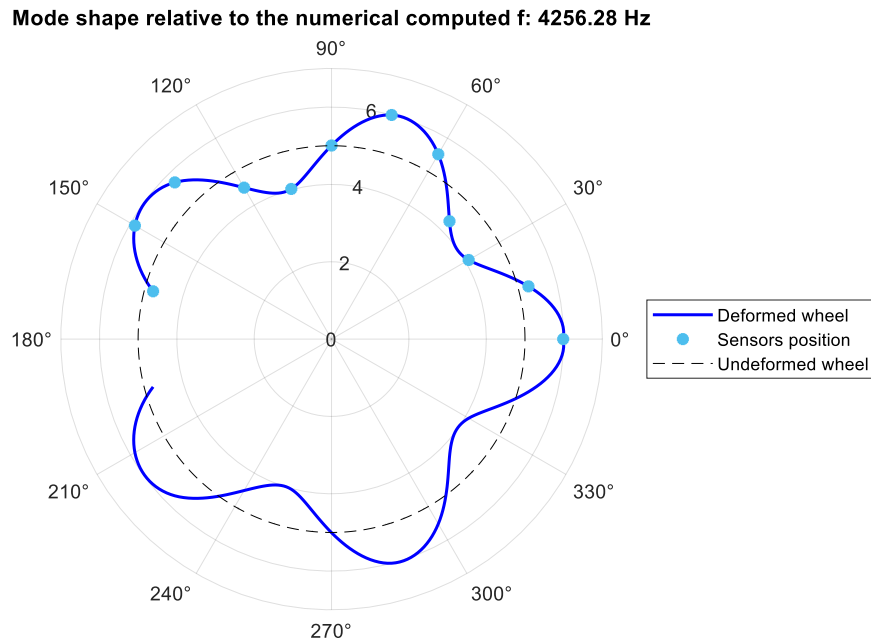


Figure 39: mode shape associated with the fourth natural frequency